Free vibration of sigmoid functionally graded plates using the dynamic stiffness method and the Wittrick-Williams algorithm

M.I. Ali[a], M.S.Azam[a], V. Ranjan[b], J.R. Banerjee[c]*

[a]Department of Mechanical Engineering, Indian Institute of Technology, Dhanbad-826004, Jharkhand, India

[b]Department of Mechanical and Aerospace Engineering,
Bennett University, Greater Noida-201310, Uttar Pradesh, India

[c]Department of Mechanical Engineering and Aeronautics,
City, University of London, Northampton Square, London EC1V 0HB, UK

Abstract

In this paper, the free vibration characteristics of Sigmoid Functionally Graded Material (S-FGM) Levy-type plates are investigated by developing the Dynamic Stiffness Method (DSM) through the application of the Wittrick-Williams algorithm, as solution technique. Kirchoff-Love Plate Theory (KLPT) and Hamilton principle are utilised to derive the governing equation of motion and associated natural boundary conditions. Based on two power-law distribution functions, the material properties are gradually varied along the thickness direction. Using the proposed theory, a substantial number of numerical examples showing the natural vibration characteristics of plates made of sigmoid functionally graded material are illustrated to demonstrate the accuracy of the method. Some numerical results are compared with published results and found to be in excellent agreement. An extensive investigation is carried out and the results are examined and discussed in detail. The variations of material properties such as the Young's modulus ratio and density ratio are seen to affect the natural frequencies of S-FGM plates significantly. The proposed method is not only accurate but also, quite simple and straightforward to compute the natural frequencies and mode shapes of S-FGM plates. The results presented can be used as benchmark solution for further investigation of FGM plates.

Keywords

Dynamic Stiffness Method; Two Power-law Functions; Wittrick-Williams Algorithm; Sigmoid Functionally Graded Material.

---

*Corresponding author.
E-mail address: j.r.banerjee@city.ac.uk (J.R. Banerjee).

1. Introduction

Functionally graded materials (FGM) are in general microscopically non-homogeneous composites in which the material properties vary continuously and smoothly along some specified directions to achieve desired characteristics or functionality [1, 2]. Material scientists in Japan appear to be the first who conceived the concept of FGM in the early 1980s [3]**.** FGM is generally constructed to operate in a high thermal environment and consists of a combination of ceramic and metal in which ceramic provides high thermal resistance, and the metal resists large stresses [4,5]. Continuous and smooth variation of the volume fractions of the two or more constituent materials in FGM eliminates the debonding between the interfaces under extreme loading conditions unlike conventional laminated composite materials. Thus, FGM is being used in aerospace industry along with a number of other applications in engineering fields, such as, in nuclear reactors, optics, automobile, electronics, energy sources, biomedical, chemical, shipbuilding industry, amongst others. Computer circuit industry also makes wide use of FGM. Of late, it is being used in smart structures, such as, Functionally Graded Piezoelectric Materials (FGPM) [6,7]. An FGM plate is generally modelled by Power law (P-FGM), Exponential law (E-FGM) and Sigmoid law (S-FGM) distributions. Power-law distribution has been used by Jin and Paulino [8]; Yang and Munz [9]; Talha and Singh [10]; Uymaz et al. [11]; Atmane et al. [12] ; Zhao et al. [13]; Neves et al. [14] whereas exponential law distribution features in the works of Jin and Batra [15]; Delale and Erdogan [16]; Gu and Asaro [17]; Erdogan and Wu [18]; Jin and Noda [19]; Erdogan and Chen [20]. These investigators discussed the effects of the variation of material properties on the stress distribution and vibration characteristics of FGMs. However, it should be recognised that the stress concentrations somehow exist in one of the interfaces in both power-law and exponential law distributions. This is because even though the material is continuous, it rapidly changes its properties. To circumvent this problem, Chung and Chi [21] proposed a sigmoid functionally graded plate (S-FGM) where two power-law functions are used to achieve a new volume fraction. The merit of the sigmoid functionally graded plate lies in the fact that it can reduce stress concentration more effectively. Stress concentrations do not occur to any appreciable extent at the interface of the materials when the FGM plate is modelled by sigmoid law distributions. Chi and Chung [22] highlighted that the stress intensity factors of a cracked FGM plate can decrease substantially by using sigmoid law distribution. Additionally, they investigated the mechanical behavior of rectangular FGM plates under transverse load and illustrated the variations of the volume fraction of the constituents of the material along the transverse direction when using a power law, exponential law and sigmoid law distribution [23].

Many researchers have studied the dynamic behavior and vibration characteristics of Sigmoid Functionally Graded Material (S-FGM) plates using different plate theories as explained below. Jung et al. [24] studied the free and forced vibration of S-FGM plates embedded on Pasternak's elastic foundation based on the four-variable refined Higher Order Shear Deformation Plate Theory. Fazzolari [25] focused attention on the modal characteristics of both P-FGM and S-FGM plates subjected to ultra-high temperature environment by using Hierarchical Higher order Equivalent Single layer Plate Theory. Jung et al. [26] computed the deflection and eigenvalue of S-FGM microplates resting on an elastic foundation by the modified couple stress theory. Wang and Zu [27] presented large amplitude frequency response of S-FGM plate containing porosity, based on Von Karman nonlinear plate theory. In their work, the volume fraction of the constituents containing porosity varied along thickness direction according to

the sigmoid law distribution. Wang and Zu [28] reported a nonlinear vibration analysis of longitudinally moving S-FGM plate based on the Von Karman nonlinear plate theory. Apart from the literature available on the study of S- FGM plates, there are several other publications on the study of the sigmoid functionally graded beam as well. For instance, the analysis undertaken by Ben-Oumrane et al. [29] on the static and bending analysis of S-FGM rectangular beam under uniformly distributed transverse load subjected to simply supported boundary conditions based on Aydogdu model is an appropriate example. Ebrahimi and Barati [30] reported the wave propagation in nanoscales S-FGM beams embedded in elastic foundation subjected to longitudinal magnetic field by nonlocal strain gradient theory and the Euler–Bernoulli beam model.

At this juncture, it is to be pointed out that the mid-surface and neutral surface in a homogeneous isotropic plate generally coincide whereas in the case of the FGM plate, they do not. The reason for the non- coincidence in the latter is that the elastic properties vary along the transverse direction. In the context of the FGM , many researchers (Yin et al. [31] ; Kim and Lee [32]; Lee et al. [33]; Zhang [34]; Zhang and Zhou [35]) employed the approach of the neutral surface variation in the constitutive equation of the FGM plate. Consequently, they found that by selecting a proper reference plane, the coupling between the membrane and curvature modes can be eliminated. Furthermore, Abrate [36] took up the issue for the mechanics of functionally graded plates and elaborated on their tendency to act as a homogeneous and isotropic plate if the new reference plane is properly selected. In addition, Han et al. [37] carried out the dynamic instability analysis of sigmoid FGM plates considering physical neutral surface resting on Pasternak elastic foundations based on four-variable refined plate theory. On the other hand, Eltaher et al. [38] determined the physical neutral axis and obtained the eigenvalues of modified FG nanobeams on the basis of Euler–Bernoulli beam theory. They discussed the effects of the nonlocal parameter, elasticity ratio and density ratio on the eigenvalues of macro and nano beams**.** Zhang [39] presented the modelling of functionally graded beams based on higher order shear deformation theory (HSDT) and by properly accounting for the neutral surface. Ding et al. [40] discussed the geometrical nonlinear vibration analysis of FG Euler Bernoulli beam in tandem with neutral surface lying on the elastic foundation by using Von Kármán's plate theory.

In the current work, the computation of eigenvalues and eigenmodes for the natural vibration of sigmoid functionally graded plates by an exact method known as the Dynamic Stiffness method (DSM) is proposed. The DSM is a powerful analytical method for free vibration analysis of structures and is well-known as a better alternate to the Finite Element Method [FEM]. The DSM has found wide applications and acceptance in recent years. It is based on exact shape functions, obtained from the exact solution of the governing differential equations. Hence, it is also called an exact method [41]. Since, the results from this method does not depend on the number of elements, it ensures much better accuracy and computational efficiency[42] when compared with the finite element method (FEM). When dealing with high frequency vibration and when better accuracy is required, the use of the DSM is most effective. The basic building block in DSM is the frequency dependent dynamic stiffness matrix that comprises both mass and stiffness properties of individual elements. Unlike the FEM, there are no separate mass and stiffness matrices for each element in the DSM. FEM deals with linear eigenvalue problems whereas DSM deals with nonlinear eigenvalue problems. The elements of DSM are generally transcendental functions of the frequency and the application of Wittrick-Williams (W-W) algorithm as solution technique is extremely advantageous [43].

During our research, we carried out a detailed literature review and found that the papers published by Banerjee and his co-workers [44–48] and Ghorbel et al [49, 50] are probably the most notable contributions in recent years dealing with the free vibration characteristics of isotropic and orthotropic plates using DSM. Others researchers namely Boscolo and Banerjee [51–53]; Liu and Banerjee [54, 55]; Fazzolari et al. [56]; Thinh et al. [57] successfully employed the DSM with the application of the Wittrick-Williams algorithm to compute the eigenvalue and eigenvectors of composite plates. Subsequent developments followed. For instance, Pagani et al.[58] formulated the DSM with the application of the Wittrick–Williams algorithm in computing the eigenvalue of composite beams subjected to different boundary conditions whereas Marjanović et al. [59] formulated the DSM for computing the eigenvalue of transversely isotropic multilayered rectangular plates subjected to different boundary conditions. The authors of [59] included the effects of various parameters such as face to core module ratio, face to core thickness ratio and shear deformation on the free vibration behaviour of sandwich plates. Employing a different approach in contrast to the previous ones, Kolarevic et al. [60] utilized the superposition technique and projection method to develop the DSM of rectangular plate assemblies. They used boundary layer function to change the three coupled Euler-Lagrange equations of motion into two uncoupled equations of motion. By contrast, Gupta and Talha [61] examined the influence of porosity on the flexural response of gradient plate using non-polynomial higher-order shear and normal deformation theory. The results for the degenerate case when an orthotropic or functionally graded or porous plate boils down to an isotropic plate as the limiting case, can be compared with the ones reported by Leissa in his classic paper [62].

It is noted, after carefully going through the pertinent literature that various researchers have used various methods [63-66] for computing the eigenvalues and eigenmodes of FGM plates, but to the best of the authors' knowledge, research leading to the analysis of free vibration characteristics of sigmoid functionally graded plate using the DSM has apparently not taken place, prior to the current one. Consequently, the novelty of the present work is principally the use of the DSM with the application of the Wittrick-Williams algorithm to determine the eigenvalues and eigenmodes of the sigmoid functionally graded plates and generate some new knowledge. The results obtained from the DSM are compared with published results for some cases. The effects of different parameters of the S-FGM plate on its free vibration characteristics are discussed in detail. It is observed that the results obtained from DSM are highly accurate and can be used as a benchmark solution for further research on S-FGM plates.

The layout of the rest part of the paper is as follows. Following this section on introduction, section 2 describes the mathematical modelling for the sigmoid functionally graded plate considering the neutral surface. The formulation of DSM for a Levy type S- FGM plate based on Kirchhoff-Love plate theory is outlined in section 3. The assembly procedure for the DSM and application of the Wittrick–Williams algorithm are presented in section 4. Section 5 describes a comparative study and a parametric investigation showing the effects of material properties on the frequency parameters of S-FGM plates. The conclusions of the investigation are presented in section 6.

2. Theory

2.1 Mathematical modelling for sigmoid functionally graded plate

In Fig. 1, an S-FGM plate which is an amalgamation of metal and ceramic is shown. The plate has a length L, width b and thickness h. The S-FGM plate comprises pure ceramic and pure metal

on the upper and the lower surfaces, respectively. The material density $\rho(z_{ms})$ and Young's modulus $E(z_{ms})$ vary continuously and smoothly in the thickness direction by two power-law functions (sigmoid law). Note that the suffices *ms* and *ns* in this paper indicate middle surface and neutral surface of the plate, respectively. Poisson's ratio is assumed to be constant because the influence of the Poisson's ratio (which has a value of around 0.3 and does not vary markedly in metal and ceramic) on the behaviour of the FGM plate seems to be much less signifant than that of the Young's modulus and density. Several researchers have employed the power law, exponential law and sigmoid law to define the volume fractions, but in the present study as already mentioned sigmoid law is used to define the volume fraction of the material.

The sigmoid law requirement is very important because due to this assumption, the stress concentration more or less disappears at the interface of the materials of an S-FGM plate. The variation of volume fractions $V_f(z_{ms})$ of the constituents of the S-FGM plate through the thickness direction is given by two power law functions [21].

$$\left.\begin{aligned} V_f{}^{(1)}(z_{ms}) &= \tfrac{1}{2}\left(\tfrac{h/2+z_{ms}}{h/2}\right)^k \quad \text{for} \quad -h/2 \le z_{ms} \le 0 \\ V_f{}^{(2)}(z_{ms}) &= 1-\tfrac{1}{2}\left(\tfrac{h/2-z_{ms}}{h/2}\right)^k \quad \text{for} \quad 0 \le z_{ms} \le h/2 \end{aligned}\right\} \quad (1)$$

where k denotes the non-negative material gradient index that controls the volume fraction of the material in the thickness direction.

By using the rule of mixture, the material properties (P) are graded through the thickness direction according to the Voigt model [67-74] as follows. (Note that Ref. [74] highlighted the advantages and disadvantages of various models, e.g. Reuss, Voigt and Mori-Tanaka model.)

$$\left.\begin{aligned} P_1(z_{ms}) &= V_f{}^{(1)}(z_{ms})P_c + [1-V_f{}^{(1)}(z_{ms})]P_m \quad \text{for} \quad -h/2 \le z_{ms} \le 0 \\ P_2(z_{ms}) &= V_f{}^{(2)}(z_{ms})P_c + [1-V_f{}^{(2)}(z_{ms})]P_m \quad \text{for} \quad 0 \le z_{ms} \le h/2 \end{aligned}\right\} \quad (2)$$

where $P_1(z_{ms})$ and $P_2(z_{ms})$ represents the typical material properties such as Young's modulus (E), material density (ρ) and Poisson's ratio (μ). P_c and P_m are the material properties of the ceramic and metal, respectively.

The Young's modulus and material density for the S-FGM plate vary along the transverse direction by the two power-law distribution function as shown in Fig. 2 (a) and (b), respectively.

2.2 Kirchoff- Love plate theory

According to Kirchoff- Love plate theory, the deformation field of an arbitrary point (x, y, z_{ms}) at any arbitrary time 't' can be expressed as [62]

$$\left.\begin{aligned} u(x,y,z_{ms},t) &= u_0(x,y,t) - z_{ms}\varphi_y(x,y,t) \\ v(x,y,z_{ms},t) &= v_0(x,y,t) - z_{ms}\varphi_x(x,y,t) \\ w(x,y,z_{ms},t) &= w_0(x,y,t) \end{aligned}\right\} \quad (3)$$

where, u, v, w are the displacement field of a point on the middle plane of the plate in the respective x, y, z direction, u_0 and v_0 are the membrane displacements and w_0 is the transverse

displacement of a point on the middle plane, φ_x and φ_y are the bending rotations about the x and y axes, respectively.

The strain related to the above displacement field can be expressed as

$$\{\varepsilon\} = \begin{Bmatrix} \varepsilon_{xx} \\ \varepsilon_{yy} \\ \gamma_{xy} \end{Bmatrix} = \{\varepsilon^0{}_{xx}\} - z_{ms}\{k^0{}_{xx}\} \tag{4}$$

in which $\varepsilon^0{}_{xx}$ and $k^0{}_{xx}$ are the in-plane strains, and bending and twisting curvatures, respectively.

2.3 Neutral Surface

Unlike homogeneous isotropic plates, the neutral surface of an S-FGM plate does not coincide with the mid surface of the plate. This is due to the variation of material properties along the thickness direction of the plate. Thus, neutral surface of an S-FGM plate will no longer be at the mid-surface. Figure 3 shows the position of neutral surface and middle surface for an S-FGM plate which are separated by a distance 'a'.

As the neutral surface takes a new coordinate system, its position can be defined as follows.

$$z_{ms} = z_{ns} + a \tag{5}$$

If the governing differential equation is based on the neutral surface, the S-FGM plate can be handled relatively easily because the coupling between the membrane and bending deformation in Kirchoff-Love plate theory will not be present.

The displacement fields which account for the position of the neutral surface are given below.

$$\left.\begin{aligned} u &= -z_{ns}\frac{\partial w}{\partial x} = -(z_{ms} - a)\frac{\partial w}{\partial x} \\ v &= -z_{ns}\frac{\partial w}{\partial y} = -(z_{ms} - a)\frac{\partial w}{\partial y} \\ w &= w_0(x, y, t) \end{aligned}\right\} \tag{6}$$

The expressions for strain related to the above displacement field can be written as

$$\{\varepsilon\} = \begin{Bmatrix} \varepsilon_{xx} \\ \varepsilon_{yy} \\ \gamma_{xy} \end{Bmatrix} = -z_{ns}\begin{Bmatrix} \frac{\partial^2 w}{\partial x^2} \\ \frac{\partial^2 w}{\partial y^2} \\ 2\frac{\partial^2 w}{\partial xy} \end{Bmatrix} \tag{7}$$

In Eq. (7), ε_{xx} and ε_{yy} are normal strains and γ_{xy} is the shearing strain, respectively.

From the generalized Hooke's law, the stress is related to strain as

$$\sigma = [Q]\{\varepsilon\}$$

$$\begin{Bmatrix} \sigma_{xx} \\ \sigma_{yy} \\ \tau_{xy} \end{Bmatrix} = \begin{bmatrix} Q_{11} & Q_{12} & 0 \\ Q_{21} & Q_{22} & 0 \\ 0 & 0 & Q_{66} \end{bmatrix} \begin{Bmatrix} \varepsilon_{xx} \\ \varepsilon_{yy} \\ \gamma_{xy} \end{Bmatrix} \tag{8}$$

where σ_{xx}, σ_{yy} and τ_{xy} are the normal and shear stresses, respectively.

The elastic constants ($Q = Q_{ij}$) can be expressed as

$$Q_{ij} = \frac{E(z_{ns})}{1-\mu^2}\begin{bmatrix} 1 & \mu & 0 \\ \mu & 1 & 0 \\ 0 & 0 & \frac{1-\mu}{2} \end{bmatrix} \tag{9}$$

where (i, j =1, 2, 6) and μ is the Poisson's ratio already defined before.

The neutral surface is the surface in the cross-section of the plate where the material of the plate is not under any stress. The position of the neutral surface can be calculated by putting the total axial forces at the cross-section of the plate to zero, i.e

$$\sum F_x = \int_{-h/2-a}^{h/2-a} \sigma_{xx}\, dA = 0 \tag{10}$$

where $dA = b dz_{ns}$

Substituting Eq. (7) into Eq. (10) leads to

$$b \int_{-h/2-a}^{h/2-a} E(z_{ns}) z_{ns} \frac{\partial^2 w}{\partial x^2} d\, z_{ns} = 0 \tag{11}$$

where b is the width of the plate.

As the material properties vary along the transverse direction by two power-law functions, the above expression can be written as:

$$b\left[\int_{-h/2-a}^{0} E_1(z_{ns}) z_{ns} \frac{\partial^2 w}{\partial x^2} dz_{ns} + \int_{0}^{h/2-a} E_2(z_{ns}) z_{ns} \frac{\partial^2 w}{\partial x^2} dz_{ns}\right] = 0 \tag{12}$$

By varying the integration from z_{ns} to z_{ms}, Eq. (12) is written as

$$b\left[\int_{-h/2}^{0} E_1(z_{ms})(z_{ms} - a) \frac{\partial^2 w}{\partial x^2} dz_{ms} + \int_{0}^{h/2} E_2(z_{ms})(z_{ms} - a) \frac{\partial^2 w}{\partial x^2} dz_{ms}\right] = 0 \tag{13}$$

This implies,

$$b\left[\int_{-\frac{h}{2}}^{0} E_1(z_{ms}) z_{ms} dz_{ms} - a\int_{-\frac{h}{2}}^{0} E_1(z_{ms}) dz_{ms} + \int_{0}^{\frac{h}{2}} E_2(z_{ms}) z_{ms} dz_{ms} - a\int_{0}^{\frac{h}{2}} E_2(z_{ms}) dz_{ms}\right] = 0$$

Therefore, the location of neutral surface can be determined from the following equation

$$a = \frac{\int_{-h/2}^{0} E_1(z_{ms}) z_{ms} dz_{ms} + \int_{0}^{h/2} E_2(z_{ms}) z_{ms} dz_{ms}}{\int_{-h/2}^{0} E_1(z_{ms}) dz_{ms} + \int_{0}^{h/2} E_2(z_{ms}) dz_{ms}}$$

or,

$$a = \frac{\frac{h}{4}(E_c - E_m) + \frac{h(E_m - E_c)}{2(k+2)(k+1)}}{(E_c + E_m)} = \frac{h\left(\frac{1}{4}(E_{rat} - 1) + \frac{(1 - E_{rat})}{2(k+2)(k+1)}\right)}{(E_{rat} + 1)} \tag{14}$$

where

$$E_{rat} = E_c / E_m \tag{14a}$$

One can notice from the Eq. (14) that the nondimensional shift (*a/h*) of the S-FGM plate depends upon the value of Young's modulus ratio (E_c/E_m) and the material gradient index (*k*). The influence of the material gradient index (*k)* on the non-dimensional shift (*a/h*) for different E_c/E_m is shown in Fig. 4. It is observed from Fig. 4 that when $E_c/E_m = 1$, the non-dimensional shift (*a/h*) is zero for the values of material gradient indices (*k* =0, 0.1, 0.2, 0.5, 1, 2, 5, 10, 20). This is due to the fact that the neutral surface and mid surface of the plate coincide and subsequently, the plate behaves like a homogeneous isotropic plate. In addition, it is apparent from Fig. 4 that when $E_c/E_m \neq 1$, the non-dimensional shift increases significantly for values of $k< 2$ and becomes almost constant when *k* increases beyond the value of 2 (i.e. the value of non-dimensional shift (*a/h*) becomes an asymptotic curve as the value of *k* increases for a specific value of E_c/E_m). It is found that as the ratio E_c/E_m increases, the neutral surface of the S-FGM plate shifts from the mid-surface and approaches towards the upper surface which is rich in ceramic. This happens mainly because the ceramic constituent of the S-FGM plate has higher stiffness than the metallic constituent.

The material property functions and volume fractions $V_f(z_{ns})$ of the different types of FGM plates based on the neutral surface are shown in Table 1 [24].

Considering the shift in the neutral surface, the governing equation of motion and associated natural boundary conditions of the S-FGM plate are obtained using Hamilton's principle, as shown below.

Governing differential equation:

$$D^*\left(\frac{\partial^4 w_0}{\partial x^4} + 2\frac{\partial^4 w_0}{\partial x^2 \partial y^2} + \frac{\partial^4 w_0}{\partial y^4}\right) + I_0 \frac{\partial^2 w_0}{\partial t^2} = 0 \tag{15}$$

Natural boundary conditions:

$$\left.\begin{aligned} V_x &= -D^*\left(\frac{\partial^3 w_0}{\partial x^3} + (2-\mu)\frac{\partial^3 w_0}{\partial x \partial y^2}\right) \\ M_{xx} &= -D^*\left(\frac{\partial^2 w_0}{\partial x^2} + \mu\frac{\partial^2 w_0}{\partial y^2}\right) \end{aligned}\right\} \tag{16}$$

where V_x is the shear force (tranverse force), M_{xx} is the bending moment and D^* is the effective flexural rigidity, I_0 is inertial coefficients and μ is the Poisson's ratio for the S-FGM plate. The explicit expressions of $D^*$and I_0 used in Eq. (15) are given in Appendix A.

3. Formulation of the dynamic stiffness matrix for the S- FGM plate

The steps adopted in the formulation of the DSM for the S-FGM plate are as follows:

(*i*) The partial differential equation of motion (Eq. (15)) for the S- FGM plate is first solved by assuming harmonic oscillation, (*ii*) Next, generic boundary conditions are applied to the edges of the Levy-type S-FGM plate for both forces and displacements which are essentially the expressions of displacement, rotation, shear force and bending moment, (*iii*) Finally, the constants of integration are eliminated from the solution by establishing the relationship between the harmonically varying forces with those of the corresponding displacements to formulate the DSM.

The solution of Eq. (15) is sought in the traditional Levy form, i.e. the opposite edges of the plate are simply supported, which satisfies the boundary conditions in the following form:

$$w_0(x,y,t) = \sum_{m=1}^{\infty} W_m(x) e^{i\omega t} \sin(\alpha_m y) \tag{17}$$

where ω is the angular or circular frequency, W_m is the amplitude of $w_0(x,y,t)$ and $\alpha_{m=} \frac{m\pi}{L}$

Obviously, m is the number of half sine waves in the x -direction with L being the length of the plate.

Substituting $w_0(x,y,t)$ from Eq. (17) into Eq. (15), the following ordinary differential equation is obtained:

$$\frac{d^4W_m}{dx^4} - 2\alpha_m \frac{d^2W_m}{dx^2} + \left(\alpha_m^4 - \frac{I_0\omega^2}{D^*}\right) W_m = 0 \qquad m = 1,2,3 \dots \dots \dots \dots \dots \infty \tag{18}$$

The four roots of the auxiliary or characteristic equation of Eq. (18) are determined on the basis of the nature of the roots and clearly, there are two conditions feasible. These are

Case 1. $\alpha_m^2 \geq \omega\sqrt{\frac{\rho h}{D^*}}$ All four roots are real $(r_{1m,}\ {}_-r_{1m,}\, r_{2m,} -\ r_{2m}\ )$

$$r_{1m} = \sqrt{\alpha_m^2 + \omega\sqrt{\frac{\rho h}{D^*}}}\ , \qquad r_{2m} = \sqrt{\alpha_m^2 - \omega\sqrt{\frac{\rho h}{D^*}}} \tag{19}$$

The solution is given by:

$$W_m(x) = A_m \cosh(r_{1m}x) + B_m \sinh(r_{1m}x) + C_m \cosh(r_{2m}x) + D_m \sinh(r_{2m}x) \tag{20}$$

Case 2. $\alpha_m^2 < \omega\sqrt{\frac{\rho h}{D^*}}$, Two roots are real and two roots are imaginary

$(r_{1m,}\ {}_-r_{1m,}\, ir_{2m,} - i\, r_{2m}\ )$

$$r_{1m} = \sqrt{\alpha_m^2 + \omega\sqrt{\frac{\rho h}{D^*}}}\ , \qquad r_{2m} = \sqrt{-\alpha_m^2 + \omega\sqrt{\frac{\rho h}{D^*}}} \tag{21}$$

The solution is given by:

$$W_m(x) = A_m \cosh(r_{1m}x) + B_m \sinh(r_{1m}x) + C_m \cos(r_{2m}x) + D_m \sin(r_{2m}x) \tag{22}$$

The formulation procedure of DSM for case 2 is shown below, but for case 1 it is not presented for the sake of brevity as it is followed in a similar manner.

The bending rotation (ϕ_y), shear force (V_x) and bending moment (M_{xx}) can be obtained from the known displacement w_0 (Eqs.(17) and (22)) resulting in the following expressions.

$$\phi_{ym}(x,y) = \varphi_{ym}(x)\sin(\alpha_m y) = -\{r_{1m}A_m \sinh(r_{1m}x) + r_{1m}B_m \cosh(r_{1m}x) - r_{2m}C_m \sin(r_{2m}x) + r_{2m}D_m \cos(r_{2m}x)\sin(\alpha_m y)\} \quad (23)$$

$$V_{xm}(x,y) = v_{xm}(x)\sin(\alpha_m y) = -D^*\{A_m\big(r_{1m}{}^3 - (2-\mu)\alpha_m{}^2 r_{1m}\big)\sinh(r_{1m}x) + B_m\,(r_{1m}{}^3 - (2-\mu)\alpha_m{}^2 r_{1m})\cosh(r_{1m}x) + C_m(r_{2m}{}^3 + (2-\mu)\alpha_m{}^2 r_{2m}\big)\sin(r_{2m}x) - D_m(r_{2m}{}^3 + (2-\mu)\alpha_m{}^2 r_{2m})\cos(r_{2m}x))\sin(\alpha_m y)\} \quad (24)$$

$$M_{xx_m}(x,y) = m_{xx_m}(x)\sin(\alpha_m y) = -D^*\{A_m(r_{1m}{}^2 - \mu\,\alpha_m{}^2)\cosh(r_{1m}x) + B_m(r_{1m}{}^2 - \mu\,\alpha_m{}^2)\sinh(r_{1m}x) - C_m(r_{2m}{}^2 + \mu\,\alpha_m{}^2)\cos(r_{2m}x) - D_m(r_{1m}{}^2 + \mu\,\alpha_m{}^2))\sin(r_{2m}x)\sin(\alpha_m y)\} \quad (25)$$

The generalized boundary conditions for displacements at both ends of the FGM plate as shown in Fig. 5 are:

$$\text{At} \quad \begin{matrix} x = 0 & W_m = W_a; & \varphi_{ym} = \varphi_{ya} \\ x = b & W_m = W_b; & \varphi_{ym} = \varphi_{yb} \end{matrix} \quad (26)$$

Similarly, generalized boundary conditions for forces at both ends of the FGM plate as shown in Fig. 5 are:

$$\text{At} \quad \begin{matrix} x = 0 & V_{xm} = -V_a; & M_{xx_m} = -M_a \\ x = b & V_{xm} = V_b; & M_{xx_m} = M_b \end{matrix} \quad (27)$$

By applying boundary conditions of Eq. (26) for displacement given by Eqs. (22) and (23), the following matrix relationship is obtained as.

$$\begin{bmatrix} W_a \\ \varphi_{y_a} \\ W_b \\ \varphi_{y_b} \end{bmatrix} = \begin{bmatrix} 1 & 0 & 1 & 0 \\ 0 & -r_{1m} & 0 & -r_{2m} \\ C_{h_1} & S_{h_1} & C_2 & S_2 \\ -r_{1m}S_{h_1} & -r_{1m}C_{h_1} & r_{2m}S_2 & -r_{2m}C_2 \end{bmatrix} \begin{bmatrix} A_m \\ B_m \\ C_m \\ D_m \end{bmatrix} \quad (28)$$

or,

$$\mathbf{X} = \mathbf{BC} \quad (29)$$

where

$$C_{h_1} = \cosh(r_{1m}b), \quad S_{h_1} = \sinh(r_{1m}b) \quad C_1 = \cos(r_{1m}b), \quad S_1 = \sin(r_{1m}b)$$
$$C_{h_2} = \cosh(r_{2m}b), \quad S_{h_2} = \sinh(r_{2m}b) \quad C_2 = \cos(r_{2m}b), \quad S_2 = \sin(r_{2m}b) \quad (30)$$

Similarly, by applying the boundary conditions of Eq. (27) for forces given by Eqs. (24) and (25), the following relationship matrix is obtained.

$$\begin{bmatrix} V_a \\ M_a \\ V_b \\ M_b \end{bmatrix} = \begin{bmatrix} 0 & R_1 & 0 & R_2 \\ L_1 & 0 & L_2 & 0 \\ -R_1 S_{h_1} & -R_1 C_{h_1} & R_2 S_{_2} & -R_2 C_{_2} \\ -L_1 C_{h_1} & -L_1 S_{h_1} & -L_2 C_{_2} & -L_2 S_{_2} \end{bmatrix} \begin{bmatrix} A_m \\ B_m \\ C_m \\ D_m \end{bmatrix} \tag{31}$$

or

$$\mathbf{F} = \mathbf{LC} \tag{32}$$

where

$$R_i = D^*(-1)^{i+1}\{r_{im}^3 - (2-\mu)\alpha^2 r_{im}\}; \qquad L_i = D^*(-1)^{i+1}(r_{im}^2 - \mu\alpha^2) \tag{33}$$

with $i = 1, 2$

The relationship between the forces and displacements can now be expressed as

$$\mathbf{F} = \mathbf{KX} \tag{34}$$

where $\mathbf{K}$ is the dynamic stiffness matrix given by

$$\mathbf{K} = \mathbf{LB}^{-1} \tag{35}$$

The six independent terms $s_{vv}, s_{vm}, f_{vv}, f_{vm}, s_{mm}, f_{mm}$ of the 4×4 symmetric dynamic stiffness form the fundamental basis of the analysis as expressed below.

$$\mathbf{K} = \begin{bmatrix} s_{vv} & s_{vm} & f_{vv} & f_{vm} \\ & s_{mm} & -f_{vm} & f_{mm} \\ & Sym & s_{vv} & -s_{vm} \\ & & & s_{mm} \end{bmatrix} \tag{36}$$

The explicit expressions for each of the terms of the dynamic stiffness matrix **K** are obtained by using symbolic algebra through the application of Matlab and they are given in Appendix B.

4. Assembly procedure for DSM

Plate structures may be subdivided into many elements or substructures for which each can be represented by the above DSM formulation. The elemental dynamic stiffness matrix (**K**) as expressed in Eq. (36) is the basic requirement to compute the exact eigenvalues of the S-FGM Levy-type plate. Therefore, global DSM for the S-FGM plate structure can be assembled directly from the assembly of several elements. A solution for natural frequencies to any desired accuracy can be achieved even by using a single DS element which of course, is not possible in FEM. Unlike the FEM, DS elements here do not have nodal points but have nodal lines at the interface. The assembly procedure for DSM of S-FGM plate is carried out in the same manner as it is performed in the FEM. The assembly procedure of the DSM is shown in Fig. 6. The overall global master matrix will always be a banded matrix as in the case of FEM [44].

4.1 Boundary conditions for S-FGM plate

The applications of boundary conditions to restrain any degrees of freedom in DSM are similar to that of FEM and usually the penalty method is employed. This method generally suppresses the degree of freedom (DOF) by attaching a very large stiffness to the appropriate term on the leading diagonal of the assembled dynamic stiffness matrix.

The following procedure is used to apply the boundary conditions.

- Free (F): no penalty is applied.
- Simply supported (S): transverse displacement (W) is penalized.
- Clamped (C): transverse displacement (W) and bending rotation (φ_y) are penalized.

4.2 Application of the Wittrick –Williams algorithm

The Wittrick–Williams algorithm [43] is generally applied as solution technique for free vibration analysis of structures or structural elements using DSM. The global dynamic stiffness matrix of the plate structure contains the transcendental function of frequency for which the Wittrick–Williams algorithm is considered to be the best way to determine the natural frequencies without missing any. The algorithm takes into consideration the Sturm sequence property of the dynamic stiffness matrix which guarantees that all naural frequencies are computed. The computational steps involved are shown in Fig. 7 using a flow chart.

5. Results and discussion

In order to compute the eigenvalues (natural frequencies) and eigenvectors (mode shapes) of S-FGM plates, a MATLAB program was developed using the above theory. In this section, results are presented and the significances of aspect ratio (L/b), material gradient index (k), boundary conditions and material properties on the eigenvalues of the S-FGM plate are discussed. Table 2 shows properties of the material constituents of the functionally graded plates reported by different researchers in the literature to investigate their free vibration characteristics. By and large, these properties [61] are used in obtaining the results of this paper.

The effect of different materials on the eigenvalue of the S-FGM plate is first demonstrated. The variations of fundamental natural frequency parameter defined in Eq. (37) below, with the material gradient index (k) are presented in Fig. 8 for different material constituents of the S-FGM plate. For lower value of k, for example, k<2, the natural frequency decreases for all the different materials used in the analysis. However, when k increases beyond the value of 2, the decrease in the natural frequency becomes less noticeable. It is also observed from the figure that there is significant reduction in the frequency parameter for Al /Al_2O_3 plate with increasing values of k, particularly in the range $0< k <5$. This is due to the large differences in the material properties of the constituent of the S-FGM plate, especially for the density. The figure also reveals the extent of the variation of the natural frequency of the plate depending upon the type of material used. The plates having lower values of Young's modulus (e.g. ZrO2/Ti-6Al-4V) being more flexible give lower values of natural frequencies, as expected.

5.1 Analysis of isotropic and S-FGM plates - a comparative study

The natural frequency parameters for the isotropic and S-FGM plates used in the study are respectively defined in non-dimensional forms by ω^* and $\bar{\omega}$ as follows.

$$\omega^* = \omega L^2 \sqrt{\frac{\rho h}{D^*}} \quad ; \qquad \bar{\omega} = \omega \frac{L^2}{h} \sqrt{\frac{\rho_c}{E_c}} \tag{37}$$

where E_c and E_m are the modulus of elasticity and ρ_c and ρ_m are the material density of ceramic and metal of the S- FGM plate respectively.

First of all, attention is focused on the validation of results computed from the present theory. This is achieved by comparing the natural frequency parameters with the ones that are available in the literature for isotropic and S-FGM plates. A carefully selected samples of results to demonstrate the validation of results from different perspectives are given in Tables (3)-(5) for which the following material properties are used.

E_c=380 GPa; E_m = 69 GPa; ρ_c =3980 kg/m^3; $\rho_m = 2710$ kg/m^3.

Using standard notation, the number of half sine wave in the *x*-direction is represented by 'm' while the nth eigenvalue, for a certain value of m, is denoted by 'n' when presenting the results.

In the first example, see Tables 3 and 4, the natural frequency parameter (ω^*) for the first six natural frequencies of a rectangular isotropic plates for SSSS and SCSC boundary conditions computed by the present theory are compared with the published results of Boscolo and Banerjee [44] and Leissa [62]. The results are indeed in very good agreement as can be seen.

In the second example, see Table 5, the fundamental natural frequency parameter ($\bar{\omega}_1$) of a square S-FGM plate for SSSS boundary condition computed by the present theory is compared with published results [24, 64, 65, 66] for different values of *k* and length to thickness (*L/h*) ratio. The comparative results are those of Jung et al. [24], Hosseini-Hashemi et al. [64], Thai and Vo [65] and with Hosseini-Hashemi et al. [66] which are based on NTSDT, HSDT, SSDT, and, FSDT, respectively. The fundamental natural frequency computed by the present method agrees very well with published results, as can be seen in Table 5.

5.2 Analysis of S-FGM plates

Table 6 shows the first six natural frequency parameters ($\bar{\omega}$) of a rectangular Levy-type S-FGM plate based on the current theory with six common boundary conditions (SSSS, SFSS, SFSF, SFSC, SSSC and SCSC) for different values of *k*. Representative values of the aspect

ratio *L/b* =2 and and thickness to length ratio *h/L*=0.01 are used in the data when obtaining the results.

It is clear from the results in Table 6 that with increasing values of *k*, the natural frequency parameter ($\bar{\omega}$) decreases for all of the boundary conditions. This is to be expected because the S- FGM plate has smaller ceramic constituents for higher values of *k* and hence its stiffness decreases. It is also observed that the natural frequency parameters ($\bar{\omega}$) of the S-FGM plat are highest for SCSC boundary condition and lowest for SFSF boundary condition for a given value of *k*. This is because, as the constraints on the edges of the plate increases, the stiffness of the plate increases which leads to an increase in the natural frequency parameter ($\bar{\omega}$).

Four representive mode shapes of an S-FGM square plate subjected to SSSS and SSSF boundary conditions for *h/L*=0.01, *k*=0.5 are presented in Figs. 9 and 10, respectively. They follow more or less similar trends as observed in isotropic plates, but of course, the natural frequency can be markedly different.

5.3 A parametric investigation

In the next stage of the investigation, a parametric study was carried out to examine the effects of different parameters such as the aspect ratio (*L/b)*, material gradient index (*k)*, Young's modulus ratio (E_c/E_m) and the density ratio (ρ_c/ρ_m)) on the frequency parameter of the S-FGM plate.

Figures 11(a) and 11(b) illustrate the variations of the fundamental natural frequency parameter ($\bar{\omega}_1$) with respect to the change in the aspect ratio (*L/b*) for different values of *k* for SCSC and SFSF boundary conditions, respectively. Fig. 11(a) shows that with the increase in the aspect ratio (*L/b*), the fundamental natural frequency parameter ($\bar{\omega}_1$) increases for all values of *k*. For isotropic and homogeneous plates (i.e. when *k* = 0 in the current theory), similar observation was made by Leissa, see his result in Table A2 of [62]. A similar trend for the variation of ($\bar{\omega}_1$) is observed for all other boundary conditions (which are not presented here for brevity) except for the SFSF case which is shown in Fig. 11 (b) . The fundamental natural frequency parameter ($\bar{\omega}_1$) of the plate under SFSF boundary conditions decreases with the increase in the aspect ratio. This trend is same as that was found in isotropic homogeneous plates, see Table A6 of [62].

In order to ascertain the effect of different boundary conditions on the fundamental natural frequency parameter ($\bar{\omega}_1$) of the rectangular S- FGM plate, the variations of the fundamental natural frequency parameter ($\bar{\omega}_1$) with aspect ratio (*L/b*) under different boundary conditions are shown in Fig. 12. The figure shows that fundamental natural frequency parameter ($\bar{\omega}_1$) increases as the aspect ratio (*L/b*) increases for all five boundary conditions, except for the SFSF boundary condition. This is in accord with the analysis carried out by Leissa [62] for isotropic homogeneous plates. Furthermore, it is revealed in Fig. 12 that the change of the fundamental natural frequency parameter ($\bar{\omega}_1$) for the SCSC boundary condition is the highest and under SFSF it is the lowest for a given (*L/b*) value. The fundamental natural frequency parameter ($\bar{\omega}_1$) of SCSC boundary condition has the highest value, and SFSF has the lowest value compared to the other boundary conditions considered in the analysis, as expected [62].

Figures 13 (a) and (b) illustrate the variations that occur in the fundamental natural frequency parameter ($\bar{\omega}_1$) of an S-FGM plate for the SSSS and SFSF boundary conditions, respectively due to the change in the material gradient index (*k*) for different values of the aspect ratio *L/b*. The figures show the trend in which the fundamental natural frequency parameter ($\bar{\omega}_1$) decreases with the increase in the values of *k* for any specific value of the aspect ratio *L/b*. It is also observed from the figures that there is a substantial decrease in the fundamental natural frequency parameter ($\bar{\omega}_1$) as the values of *k* approaches 5, but the decrease in the fundamental natural frequency parameter ($\bar{\omega}_1$) is not so pronounced when the values of *k* increases further. The same trends were observed for the boundary conditions vis-à-vis SFSS, SFSC, SSSC, and SCSC which are not shown here for brevity.

5.4 Effect of material properties

The influence of the material properties, namely the material density (ρ) and the Young's modulus (E) on the natural frequency parameter ($\bar{\omega}$) for the S-FGM plate is presented and discussed in this section. Using the variations in the Young's modulus ratio (E_c/E_m), while keeping material density ratio constant (i.e. $\rho_c/\rho_m = 1$) brings about subsequent variations in the natural frequency parameter ($\bar{\omega}$) of the square S- FGM plate which is illustrated in Fig. 14 for the first six modes of vibration for SCSS boundary condition. Additionally, it is noticed that with an increase in the Young's modulus ratio (E_c/E_m), the frequency parameter ($\bar{\omega}$), in general, decreases. However, this decrease in natural frequency is significant for lower values of the Young's modulus ratio, particularly when (E_c/E_m) < 5. The validity of this statement

can be established by using Eq. (37), which factors in the condition that ($\bar{\omega}$) is inversely proportional to the Young's modulus of the ceramic materials of the S-FGM plate.

Figure 15 highligths the variations in the natural frequency parameter ($\bar{\omega}$) due to the change in the material density ratio (ρ_c/ρ_m) while keeping the Young's modulus ratio constant (E_c/E_m =1) for the first six modes of vibration for SCSS boundary condition. An interpretation of the figure reveals that an increase in the frequency parameter ($\bar{\omega}$) is affected by an increase in the material density ratio (ρ_c/ρ_m). The validity of this statement can be established by using Eq. (37), which is due to the condition that ($\bar{\omega}$) is directly proportional to the material density of the ceramic materials of the S-FGM plate.

Figures 16 and 17, illustrate two different cases for the variations of material properties ratio, namely material density and Young's modulus ratio of the S-FGM plate on the fundamental natural frequency parameter ($\bar{\omega}_1$) for different values of *k* for the SCSS boundary condition. In the first case (Fig. 16), $\rho_c/\rho_m$is kept constant (i.e. $\rho_c/\rho_m = 1$), but E_c/E_m is varied between 1 and 40 and the corresponding effects on the fundamental natural frequency parameter ($\bar{\omega}_1$) are presented. Simultaneously, it is also noted that with an increase in E_c/E_m, there is a decrease in the fundamental natural frequency parameter ($\bar{\omega}_1$). Moreover, from the figure, it is noted that the fundamental natural frequency parameter ($\bar{\omega}_1$) decreases quite drastically when the value of E_c/E_m lies between 1 and 10. However, when E_c/E_m increases beyond 10, there is much less decrease in the fundamental natural frequency parameter ($\bar{\omega}_1$).

In the second case (Fig. 17), both the Young's modulus ratio and the density ratio are assumed to be the same, i.e. $E_c/E_m = \rho_c/\rho_m$ which varies from 1 to 40 and the corresponding effects on the fundamental natural frequency parameter ($\bar{\omega}_1$) for the SCSS boundary condition are highlighted. The figure depicts the trend in which the fundamental natural frequency parameter ($\bar{\omega}_1$) decreases as the $E_c/E_m = \rho_c/\rho_m$ ratio increases. At this juncture, it must be noted that a substantial decrease in the fundamental natural frequency parameter ($\bar{\omega}_1$) is apparent for $E_c/E_m = \rho_c/\rho_m$<10 whereas less decrease is noted in the fundamental natural frequency parameter ($\bar{\omega}_1$) beyond this value, particularly for lower value of material gradient index (*k*).

The variations of the fundamental natural frequency parameter ($\bar{\omega}_1$) of the square S- FGM plate with *k* = 0.5 and *h/L* = 0.01 against ρ_c/ρ_m for different Young's modulus ratio (i.e. E_{rat}= 1, 2, 5, 10, 20, 40) for SCSS boundary condition are shown in Fig. 18.

An inspection of the Fig. 18, highlights the fact that an increase in the values of ρ_c/ρ_m results in the increase of the fundamental natural frequency parameter $(\bar{\omega}_1)$. It is also noted that the fundamental natural frequency parameter $(\bar{\omega}_1)$ increases significantly in the range of $1 \leq \rho_c/\rho_m \leq 10$. However, the increase in the fundamental natural frequency parameter $(\bar{\omega}_1)$ is not so significant when ρ_c/ρ_m increases beyond 10.

6. Conclusions

The dynamic stiffness method (DSM) is developed for the investigation of natural vibration characteristics of sigmoid FGM Levy type plate considering physical neutral surface. The DSM is proved to be efficient and accurate when computing the eigenvalue of both isotropic and S-FGM plate structures. The eigenvalues obtained by the DSM with the application of the Wittrick-Williams algorithm match very well with published results. A comprehensive set of results is presented. The results obtained by the present method for isotropic and S-FGM plates when compared with published results in the literature revealed excellent agreement. The influences of various plate parameters such as material gradient index, aspect ratio, boundary conditions and material properties on the eigenvalues of S-FGM plate are analyzed and discussed in detail. For all modes and aspect ratios, the eigenvalues decrease as the values of the material gradient index of the S- FGM plate increase. The influence of the material gradient index on the fundamental frequency is substantial for the lower value of the material gradient index. The eigenvalues increase with an increase in the aspect ratio of the plate. The eigenvalue decreases when constraints change from the clamped edge condition to free edge condition because of the decrease in stiffness. It is interesting to note that with the increase in the E_c/E_m ratio, the fundamental frequency parameter decreases but the trends are reversed with an increment in ρ_c/ρ_m. The variations of E_c/E_m and ρ_c/ρ_m substantially affect the natural frequency and cannot be disregarded. The main contribution made in this paper is of course, the development of the DSM for S-FGM plates in order to provide highly accurate results for their eigenvalues and mode shapes. The results obtained can be used as benchmark solution to validate FEM and other approximate methods.

Appendix A

Explicit expressions for D^* and I_0 in equations (15) and (16)

$$I_0 = \int_{-h/2-a}^{h/2-a} \rho(z_{ns}) dz_{ns}$$

$$= \int_{-h/2-a}^{0} \rho_1(z_{ns}) dz_{ns} + \int_{0}^{h/2-a} \rho_2(z_{ns}) dz_{ns}$$

$$= \int_{-h/2}^{0} \rho_1(z_{ms}) dz_{ms} + \int_{0}^{h/2} \rho_2(z_{ms}) dz_{ms}$$

$$= 0.5h\rho_c \left(1 + \frac{1}{\rho_{rat}}\right)$$

where

$$\rho_{rat} = \frac{\rho_c}{\rho_m}$$

$$D^* = \int_{-h/2-a}^{h/2-a} z_{ns}^2 \, Q_{11}(z_{ns}) dz_{ns} = \int_{-h/2-a}^{0} z_{ns}^2 \, Q_{11}(z_{ns}) dz_{ns} + \int_{0}^{h/2-a} z_{ns}^2 Q_{11}(z_{ns}) dz_{ns}$$

$$= \int_{-h/2}^{0} (z_{ms} - a)^2 Q_{11}(z_{ms}) dz_{ms} + \int_{0}^{h/2} (z_{ms} - a)^2 Q_{11}(z_{ms}) dz_{ms}$$

$$= 12(D_c/E_{rat})\left(0.5 \frac{a}{h}(1 - E_{rat})\left(\frac{1}{k+2} - \frac{1}{k+1}\right) + \frac{1}{24}(1 + E_{rat}) + 0.5 \left(\frac{a}{h}\right)^2 (1 + E_{rat}) + 0.25 \frac{a}{h} (1 - E_{rat})\right)$$

where

$D_c = \frac{E_c h^3}{12(1-\mu^2)}$ is the flexural rigidity of the ceramic material and $E_{rat} = \frac{E_c}{E_m}$

Appendix B

Explicit expressions for the dynamic stiffness elements of equation (36)

$$s_{mm} = (L_1 - L_2)(r_{1m}C_{h_1}S_2 - r_{2m}C_2S_{h_1})/\nabla,$$
$$s_{vv} = (r_{2m}R_1 + r_{1m}R_2)(r_{2m}C_{h_1}S_2 + r_{1m}C_2S_{h_1})/\nabla,$$
$$s_{vm} = -(r_{2m}(R_1(C_2{}^2 - C_2C_{h_1} + S_2{}^2) - R_2S_2S_{h_1}) - r_{1m}(R_1S_2S_{h_1} - R_2((C_2 - C_{h_1})C_{h_1} + S_{h_1}{}^2))/\nabla,$$
$$f_{mm} = (L_2 - L_1)(r_{1m}S_2 - r_{2m}S_{h_1})/\nabla,$$
$$f_{vv} = (r_{1m}R_2 - r_{2m}R_1)(r_{2m}S_2 + r_{1m}S_{h_1})/\nabla,$$
$$f_{vm} = (C_2 - C_{h_1})(r_{2m}R_1 - r_{1m}R_2)/\nabla,$$

where

$$R_i = D^*(-1)^{i+1}(r_{im}^3 - (2-\mu)\alpha^2 r_{im}); \qquad L_i = D^*(-1)^{i+1}(r_{im}^2 - \mu\alpha^2) \qquad i = 1,2$$

$$C_{h_1} = \cosh(r_{1m}b), \qquad S_{h_1} = \sinh(r_{1m}b) \qquad C_1 = \cos(r_{1m}b), \qquad S_1 = \sin(r_{1m}b)$$

$$C_{h_2} = \cosh(r_{2m}b), \qquad S_{h_2} = \sinh(r_{2m}b) \qquad C_2 = \cos(r_{2m}b), \qquad S_2 = \sin(r_{2m}b)$$

and

$$\nabla = r^2{}_{1m}S_2S_{h_1} - r^2{}_{2m}S_2S_{h_1} + r_{1m}r_{2m}((C_2 - C_{h_1})^2 + S_2{}^2 - S_{h_1}{}^2)$$

References

1. L.F. Qian, R.C. Batra, Design of bidirectional functionally graded plate for optimal natural frequencies, J. Sound Vib. 280 (2005) 415–424. doi:10.1016/j.jsv.2004.01.042.
2. D.Y. Liu, C.Y. Wang, W.Q. Chen, Free vibration of FGM plates with in-plane material inhomogeneity, Compos. Struct. 92 (2010) 1047–1051 doi:10.1016/j.compstruct.2009 .10.001.
3. M. Koizumi, FGM activities in Japan, Compos. Part B Eng. 28 (1997) 1–4. doi:https ://doi.org/10.1016/S1359-8368(96)00016-9.
4. S. Suresh, A. Mortensen, Functionally graded metals and metal-ceramic composites: Part 2 Thermomechanical behaviour, Int. Mater. Rev. 42 (1997) 85–116. doi:10.1179 / imr.1997.42.3.85.
5. V. Birman, L.W. Byrd, Modeling and analysis of functionally graded materials and structures, Appl. Mech. Rev. 60 (2007) 195-216. doi:10.1115/1.2777164.
6. S. Suresh, A. Mortensen, Fundamentals of functionally graded materials, Mater. Today. 1 (1998) 18. doi:10.1016/s1369-7021(98)80023-0.
7. I. Shiota, Y. Miyamoto, Functionally graded materials, in: Proc. 4th Int. Symp. Funct. Graded Mater., Elseveir, AIST Tsukuba Research center, Tsukuba, Japan, (1996) 1–803.
8. Z.-H. Jin, G.H. Paulino, Transient thermal stress analysis of an edge crack in a functionally graded material, Int. J. Fract. 107 (2001) 73–98.doi:10.1023/ A:1026583903046.
9. Y.Y. Yang, D. Munz, Stress analysis in a two materials joint with a functionally graded material, Proc. 4th Int. Symp. Funct. Graded Mater. (1997) 41–46. doi:10.1016/ B978-044482548-3/50008-1.
10. M. Talha, B.N. Singh, Static response and free vibration analysis of FGM plates using higher order shear deformation theory, Appl. Math. Model. 34 (2010) 3991–4011. doi:10.1016/j.apm.2010.03.034.
11. B. Uymaz, M. Aydogdu, S. Filiz, Vibration analyses of FGM plates with in-plane material inhomogeneity by Ritz method, Compos. Struct. 94 (2012) 1398–1405. doi:10.1016/j.compstruct.2011.11.002.
12. H. Ait Atmane, A. Tounsi, I. Mechab, E.A. Adda Bedia, Free vibration analysis of functionally graded plates resting on Winkler–Pasternak elastic foundations using a new shear deformation theory, Int. J. Mech. Mater. Des. 6 (2010) 113–121.

doi:10.1007/s10999-010-9110-x.

13. X. Zhao, Y.Y. Lee, K.M. Liew, Free vibration analysis of functionally graded plates using the element-free kp-Ritz method, J. Sound Vib. 319 (2009) 918–939. doi:10.1016/j.jsv.2008.06.025.
14. A.M.A. Neves, A.J.M. Ferreira, E. Carrera, M. Cinefra, C.M.C. Roque, R.M.N. Jorge, C.M.M. Soares, A quasi-3D hyperbolic shear deformation theory for the static and free vibration analysis of functionally graded plates, Compos. Struct. 94 (2012) 1814–1825. doi:10.1016/j.compstruct.2011.12.005.
15. Z. Jin, R.C. Batra, Stress intensity relaxation at the tip of an edge crack in a functionally graded material subjected to a thermal shock, J. Therm. Stress. 19 (1996) 317–339. doi:10.1080/01495739608946178.
16. F. Delale, F. Erdogan, The crack problem for a nonhomogeneous plane, J. Appl. Mech. 50 (1983) 609–614. doi: 10.1115/1.3167098
17. P. Gu, R.J. Asaro, Crack deflection in functionally graded materials, Int. J. Solids Struct. 34 (1997) 3085–3098. doi:10.1016/S0020-7683(96)00175-8.
18. F. Erdogan, B.H. Wu, Crack problems in fgm layers under thermal stresses, J. Therm. Stress. 19 (1996) 237–265. doi:10.1080/01495739608946172.
19. Z. Jin, N. Noda, Crack-tip singular fields in nonhomogeneous materials, J. Appl. Mech. 39 (1994) 738-740. doi:10.1115/1.2901529.
20. Y.F. Erdogan, F. Chen, Interfacial cracking of FGM metal bonds, In: Kokini, K. (Ed.), Ceramic Coating. (1998) 29–37..
21. Y.-L. Chung, S.H. Chi, The residual stress of functionally graded materials, J. Chinese Inst. Civil hydr. Eng. 13 (2001) 1-9.
22. S.H. Chi, Y.-L. Chung, Cracking in sigmoid functionally graded coating, J. Mech. 18 (2002) 41–53.
23. S.H. Chi, Y.L. Chung, Mechanical behavior of functionally graded material plates under transverse load-Part I: Analysis, Int. J. Solids Struct. 43 (2006) 3657–3674. doi:10.1016/j.ijsolstr.2005.04.011.
24. W.Y. Jung, S.C. Han, W.T. Park, Four-variable refined plate theory for forced-vibration analysis of sigmoid functionally graded plates on elastic foundation, Int. J. Mech. Sci. 111–112 (2016) 73-87. doi:10.1016/j.ijmecsci.2016.03.001.
25. F.A. Fazzolari, Modal characteristics of P- and S-FGM plates with temperature-dependent materials in thermal environment, J. Therm. Stress. 39 (2016) 854–873. doi:10.1080/01495739.2016.1189772.

26. W.Y. Jung, W.T. Park, S.C. Han, Bending and vibration analysis of S-FGM microplates embedded in Pasternak elastic medium using the modified couple stress theory, Int. J. Mech. Sci. 87 (2014) 150–162. doi:10.1016/j.ijmecsci.2014.05.025.
27. Y.Q. Wang, J.W. Zu, Large-amplitude vibration of sigmoid functionally graded thin plates with porosities, Thin-Walled Struct. 119 (2017) 911–924. doi:https://doi.org/10.1016/j.tws.2017.08.012.
28. Y.Q. Wang, J.W. Zu, Vibration characteristics of moving sigmoid functionally graded plates containing porosities, Int. J. Mech. Mater. Des. 14 (2018) 473–489. doi:10.1007/s10999-017-9385-2.
29. S. Ben-Oumrane, T. Abedlouahed, M. Ismail, B.B. Mohamed, M. Mustapha, A.B. El Abbas, A theoretical analysis of flexional bending of Al/Al2O3 S-FGM thick beams, Comput. Mater. Sci. 44 (2009) 1344–1350. doi:10.1016/j.commatsci.2008.09.001.
30. F. Ebrahimi, M.R. Barati, Flexural wave propagation analysis of embedded S-FGM nanobeams under longitudinal magnetic field based on nonlocal strain gradient theory, Arab. J. Sci. Eng. 42 (2017) 1715–1726. doi:10.1007/s13369-016-2266-4.
31. S. Yin, T. Yu, P. Liu, Free vibration analyses of FGM thin plates by isogeometric analysis based on classical plate theory and physical neutral surface, Adv. Mech. Eng. 5 (2013) 1-10. doi:10.1155/2013/634584.
32. N. Il Kim, J. Lee, Geometrically nonlinear isogeometric analysis of functionally graded plates based on first-order shear deformation theory considering physical neutral surface, Compos. Struct. 153 (2016) 804–814. doi:10.1016/j.compstruct.2016.07.002.
33. Y.H. Lee, S.I. Bae, J.H. Kim, Thermal buckling behavior of functionally graded plates based on neutral surface, Compos. Struct. 137 (2016) 208–214. doi:10.1016/j.compstruct.2015.11.023.
34. D.G. Zhang, Nonlinear bending analysis of FGM beams based on physical neutral surface and high order shear deformation theory, Compos. Struct. 100 (2013) 121–126. doi:10.1016/j.compstruct.2012.12.024.
35. D.G. Zhang, Y.H. Zhou, A theoretical analysis of FGM thin plates based on physical neutral surface, Comput. Mater. Sci. 44 (2008) 716–720. doi:10.1016/j.commatsci.2008.05.016.
36. S. Abrate, Functionally graded plates behave like homogeneous plates, Compos. Part B Eng. 39 (2008) 151–158. doi:10.1016/j.compositesb.2007.02.026.
37. S.C. Han, W.T. Park, W.Y. Jung, A four-variable refined plate theory for dynamic stability analysis of S-FGM plates based on physical neutral surface, Compos. Struct.

131 (2015) 1081–1089. doi:10.1016/j.compstruct.2015.06.025.

38. M.A. Eltaher, A.E. Alshorbagy, F.F. Mahmoud, Determination of neutral axis position and its effect on natural frequencies of functionally graded macro/nanobeams, Compos. Struct. 99 (2013) 193–201. doi:10.1016/j.compstruct.2012.11.039.
39. D.G. Zhang, Modeling and analysis of FGM rectangular plates based on physical neutral surface and high order shear deformation theory, Int. J. Mech. Sci. 68 (2013) 92–104. doi:10.1016/j.ijmecsci.2013.01.002.
40. J. Ding, L. Chu, L. Xin, G. Dui, Nonlinear vibration analysis of functionally graded beams considering the influences of the rotary inertia of the cross section and neutral surface position, Mech. Based Des. Struct. Mach. 46 (2018) 225–237. doi:10.1080/15397734.2017.1329020.
41. J.R.Banerjee, Dynamic stiffness formulation for structural elements: A general approach, Comput. Struct. 63 (1997) 101–103. doi:10.1016/S0045-7949(96)00326-4.
42. A.Y.T. Leung, Dynamic Stiffness and Substructures, Springer-Verlag, London, 1993.
43. W.H. Wittrick, F.W. Williams, A general algorithm for computing natural frequencies of elastic structures, Q. J. Mech. Appl. Math. XXIV (1971) 263–284. doi.org/10.1093/qjmam/24.3.263
44. M. Boscolo, J.R. Banerjee, Dynamic stiffness elements and their applications for plates using first order shear deformation theory, Comput. Struct. 89 (2011) 395–410. doi:10.1016/j.compstruc.2010.11.005.
45. M. Boscolo, J.R. Banerjee, Dynamic stiffness method for exact inplane free vibration analysis of plates and plate assemblies, J. Sound Vib. 330 (2011) 2928–2936. doi:10.1016/j.jsv.2010.12.022.
46. S. O.Papkov, J.R. Banerjee, A new method for free vibration and buckling analysis of rectangular orthotropic plates, J.Sound Vib. 339 (2015): 342-358. doi:10.1016/j.jsv.2014.11.007.
47. J.R. Banerjee, S.O. Papkov, X. Liu, D. Kennedy, Dynamic stiffness matrix of a rectangular plate for the general case, J. Sound Vib. 342 (2015) 177–199. doi:https://doi.org/10.1016/j.jsv.2014.12.031.
48. X. Liu, J.R. Banerjee, Free vibration analysis for plates with arbitrary boundary conditions using a novel spectral-dynamic stiffness method, Comput. Struct. 164 (2016) 108–126. doi:https://doi.org/10.1016/j.compstruc.2015.11.005.
49. O. Ghorbel, J.B. Casimir, L. Hammami, I. Tawfiq, M. Haddar, Dynamic stiffness formulation for free orthotropic plates, J. Sound Vib. 346 (2015) 361–375.

doi:https://doi.org/10.1016/j.jsv.2015.02.020.

50. O. Ghorbel, J.B. Casimir, L. Hammami, I. Tawfiq, M. Haddar, In-plane dynamic stiffness matrix for a free orthotropic plate, J. Sound Vib. 364 (2016) 234–246. doi:https://doi.org/10.1016/j.jsv.2015.11.028.
51. M. Boscolo, J.R. Banerjee, Dynamic stiffness formulation for composite Mindlin plates for exact modal analysis of structures. Part I: Theory, Comput. Struct. 96 (2012) 61-73. doi:10.1016/j.compstruc.2012.01.002.
52. M. Boscolo, J.R. Banerjee, Dynamic stiffness formulation for composite Mindlin plates for exact modal analysis of structures. Part II: Results and applications, Comput.Struct. 96 (2012) 74–83. doi:https://doi.org/10.1016/j.compstruc.2012.01.003.
53. M. Boscolo, J.R. Banerjee, Layer-wise dynamic stiffness solution for free vibration analysis of laminated composite plates, J. Sound Vib. 333 (2014) 200–227. doi:10.1016/j.jsv.2013.08.031.
54. X. Liu, J.R. Banerjee, An exact spectral-dynamic stiffness method for free flexural vibration analysis of orthotropic composite plate assemblies – Part I: Theory, Compos.Struct.132(2015)1274–1287. doi:https://doi.org/10.1016/j.compstruct.2015.07.020.
55. X. Liu, J.R. Banerjee, An exact spectral-dynamic stiffness method for free flexural vibration analysis of orthotropic composite plate assemblies– Part II: Applications,Compos.Struct.132(2015)1288–1302. doi:https://doi.org/10.1016/j.compstruct.2015.07.022.
56. F.A. Fazzolari, M. Boscolo, J.R. Banerjee, An exact dynamic stiffness element using a higher order shear deformation theory for free vibration analysis of composite plate assemblies, Compos. Struct. 96 (2013) 262–278. doi:10.1016/j.compstruct.2012.08.033.
57. T.I. Thinh, M.C. Nguyen, D.G. Ninh, Dynamic stiffness formulation for vibration analysis of thick composite plates resting on non-homogenous foundations, Compos. Struct. 108 (2014) 684–695. doi:10.1016/j.compstruct.2013.10.022.
58. A. Pagani, E. Carrera, M. Boscolo, J.R. Banerjee, Refined dynamic stiffness elements applied to free vibration analysis of generally laminated composite beams with arbitrary boundary conditions, Compos. Struct. 110 (2014) 305–316. doi:10.1016/j.compstruct.2013.12.010.
59. M. Marjanović, N. Kolarević, M. Nefovska-Danilović, M. Petronijević, Free vibration study of sandwich plates using a family of novel shear deformable dynamic stiffness

elements: limitations and comparison with the finite element solutions, Thin-Walled Struct. 107 (2016) 678–694. doi:10.1016/j.tws.2016.08.002.

60. N. Kolarevic, M. Marjanović, M. Nefovska-Danilovic, M. Petronijevic, Free vibration analysis of plate assemblies using the dynamic stiffness method based on the higher order shear deformation theory, J. Sound Vib. 364 (2016) 110–132. doi:10.1016/j.jsv.2015.11.016.
61. A. Gupta, M. Talha, Influence of porosity on the flexural and vibration response of gradient plate using nonpolynomial higher-order shear and normal deformation theory, Int. J. Mech. Mater. Des. 14 (2018) 277–296. doi:10.1007/s10999-017-9369-2.
62. A.W. Leissa, The free vibration of rectangular plates, J. Sound Vib. 31 (1973) 257–293. doi:10.1016/S0022-460X(73)80371-2.
63. A. Hasani Baferani, A.R. Saidi, E. Jomehzadeh, An exact solution for free vibration of thin functionally graded rectangular plates, Proc. Inst. Mech. Eng. Part C: J. Mech. Eng. Sci. 225 (2011) 526–536. doi:10.1243/09544062JMES2171.
64. S. Hosseini-Hashemi, M. Fadaee, S.R. Atashipour, Study on the free vibration of thick functionally graded rectangular plates according to a new exact closed-form procedure, Compos.Struct.93(2011)722–735.doi:https://doi.org/10.1016/j.compstruct. 2010.08.007.
65. H.-T. Thai, T.P. Vo, A new sinusoidal shear deformation theory for bending, buckling, and vibration of functionally graded plates, Appl. Math. Model. 37 (2013) 3269–3281. doi:https://doi.org/10.1016/j.apm.2012.08.008.
66. S. Hosseini-Hashemi, M. Fadaee, A. S.R. Atashipour, A new exact analytical approach for free vibration of Reissner–Mindlin functionally graded rectangular plates, Int. J. Mech. Sci. 53 (2011) 11-22. doi:10.1016/j.ijmecsci.2010.10.002.
67. J.H. Kim, G.H. Paulino, An accurate scheme for mixed-mode fracture analysis of functionally graded materials using the interaction integral and micromechanics models, Int. J. Numer. Meth. Eng. 58 (2003) 1457–1497. doi:https://doi.org/10.1002/nme.819.
68. L.L. Mishnaevsky, Computational Mesomechanics of Composites: Numerical Analysis of the Effect of Microstructures of Composites of Strength and damage Resistance. Wiley, London (2007)
69. R.W.Zimmerman, Behavior of the Poisson ratio of a two-phase composite material in the high-concentration limit, Appl. Mech. Rev. 47(1) (1994) 38–44. doi:https://doi.org/10.1115/1.3122819.

70. A. R. Nemati, M. J. Mahmoodabadi, Effect of micromechanical models on stability of functionally graded conical panels resting on Winkler–Pasternak foundation in various thermal environments, Arch. Appl. Mech. (2020) 883-915. doi.org/10.1007/s00419-019-01646-6

71. S. J. Singh, S. P. Harsha, Buckling analysis of FGM plates under uniform, linear and non-linear in-plane loading, J. Mech. Sc. Tech. 33 (4) (2019) 1761-1767. doi: 10.1007/s12206-019-0328-8.

72. T. Nakamura, T. Wang, S. Sampath, Determination of properties of graded materials by inverse analysis and instrumented indentation, Acta. Mater. 48 (2000) 4293–4306. doi: https://doi.org/10.1016/S1359-6454(00)00217-2.

73. A. Gupta, M. Talha, W. Seemann, Free vibration and flexural response of functionally graded plates resting on Winkler--Pasternak elastic foundations using non-polynomial higher order shear and normal deformation theory, Mech. Adv. Mat. Struct, 25(6) (2018) 523-538. doi: https://doi.org/10.1080/15376494.2017.1285459.

74. M.M. Gasik, Micromechanical modelling of functionally graded materials, Comput. Mater. Sci. 13 (1998), 42-55, doi: https://doi.org/10.1016/S0927-0256(98)00044-5.

Free vibration of sigmoid functionally graded plates using the dynamic stiffness method and the Wittrick-Williams algorithm

M.I. Ali[a], M.S.Azam[a], V. Ranjan[b], J.R. Banerjee[c]*

[a]Department of Mechanical Engineering, Indian Institute of Technology, Dhanbad-826004, Jharkhand, India

[b]Department of Mechanical and Aerospace Engineering,
Bennett University, Greater Noida-201310, Uttar Pradesh, India

[c]Department of Mechanical Engineering and Aeronautics,
City, University of London, Northampton Square, London EC1V 0HB, UK

Abstract

In this paper, the free vibration characteristics of Sigmoid Functionally Graded Material (S-FGM) Levy-type plates are investigated by developing the Dynamic Stiffness Method (DSM) through the application of the Wittrick-Williams algorithm, as solution technique. Kirchoff-Love plate theory (KLPT) and Hamilton principle are utilised to derive the governing equation of motion and associated natural boundary conditions. On the basis of two power-law distribution functions, the material properties are gradually varied along the thickness direction. Using the proposed theory, a substantial number of numerical examples showing the natural vibration characteristics of plates made of sigmoid functionally graded material are illustrated to demonstrate the accuracy of the method. Some numerical results are compared with published results and found to be in excellent agreement. An extensive investigation is carried out and the results are examined and discussed in detail. The variations of material properties such as the Young's modulus ratio and density ratio are seen to affect the natural frequencies of S-FGM plates significantly. The proposed method is not only accurate but also, quite simple and straightforward to compute the natural frequencies and mode shapes of S-FGM plates. The results presented can be used as benchmark solution for further investigation of FGM plates.

Keywords

Dynamic Stiffness Method; Two Power-law Functions; Wittrick-Williams Algorithm; Sigmoid Functionally Graded Material.

---

*Corresponding author.
E-mail address: j.r.banerjee@city.ac.uk (J.R. Banerjee).

1. Introduction

Functionally graded materials (FGM) are in general microscopically non-homogeneous composites in which the material properties vary continuously and smoothly along some specified directions to achieve desired characteristics or functionality [1, 2]. Material scientists in Japan appear to be the first who conceived the concept of FGM in the early 1980s [3]**.** FGM is generally constructed to operate in a high thermal environment and consists of a combination of ceramic and metal in which ceramic provides high thermal resistance, and the metal resists large stresses [4,5]. Continuous and smooth variation of the volume fractions of the two or more constituent materials in FGM eliminates the debonding between the interfaces under extreme loading conditions unlike conventional laminated composite materials. Thus, FGM is being used in aerospace industry along with a number of other applications in engineering fields, such as, in nuclear reactors, optics, automobile, electronics, energy sources, biomedical, chemical, shipbuilding industry, amongst others. Computer circuit industry also makes wide use of FGM. Of late, it is being used in smart structures, such as, Functionally Graded Piezoelectric Materials (FGPM) [6,7]. An FGM plate is generally modelled by Power law, Exponential law and Sigmoid law distributions. Power-law distribution has been used by Jin and Paulino [8]; Yang and Munz [9];Talha and Singh [10]; Uymaz et al. [11]; Atmane et al. [12] ; Zhao et al. [13]; Neves et al. [14] whereas exponential law distribution features in the works of Jin and Batra [15]; Delale and Erdogan [16]; Gu and Asaro [17]; Erdogan and Wu [18]; Jin and Noda [19]; Erdogan and Chen [20]. These investigators discussed the effects of the variation of material properties on the stress distribution and vibration characteristics of FGMs. However, it should be recognised that the stress concentrations somehow exist in one of the interfaces in both power-law and exponential law distributions. This is because even though the material is continuous, it rapidly changes its properties. To circumvent this problem, Chung and Chi [21] proposed a sigmoid functionally graded plate (S-FGM) where two power-law functions are used to achieve a new volume fraction. The merit of the sigmoid functionally graded plate lies in the fact that it can reduce stress concentration more effectively. Stress concentrations do not occur to any appreciable extent at the interface of the materials when the FGM plate is modelled by sigmoid law distributions. Chi and Chung [22] highlighted that the stress intensity factors of a cracked body of the FGM plate can decrease substantially by using sigmoid law distribution. In addition, they also focused their attention on the mechanical behavior of rectangular FGM plates under transverse load and illustrated the variations of the volume fraction of the constituents of the material along the transverse direction when using a power law, exponential law and sigmoid law distribution [23].

Many researchers have studied the dynamic behavior and vibration characteristics of Sigmoid Functionally Graded Material (S-FGM) plates using different plate theories as explained below. Jung et al. [24] studied the free and forced vibration of S-FGM plates embedded on Pasternak's elastic foundation based on the four-variable refined Higher Order Shear Deformation Plate Theory. Fazzolari [25] focused attention on the modal characteristics of both P-FGM and S-FGM plates subjected to ultra-high temperature environment by using Hierarchical Higher order Equivalent Single layer Plate Theory. Jung et al. [26] computed the deflection and eigenvalue of S-FGM microplates resting on an elastic foundation by the modified couple stress theory. Wang and Zu [27] presented large amplitude frequency response of S-FGM plate containing porosity, based on Von Karman nonlinear plate theory. In their work, the volume fraction of the constituents containing porosity varied along thickness direction according to

the sigmoid law distribution. Wang and Zu [28] reported a nonlinear vibration analysis of longitudinally moving S-FGM plate based on the Von Karman nonlinear plate theory. Apart from the literature available on the study of S- FGM plates, there are several other publications on the study of the sigmoid functionally graded beam as well. For instance, the analysis undertaken by Ben-Oumrane et al. [29] on the static and bending analysis of S-FGM rectangular beam under uniformly distributed transverse load subjected to simply supported boundary conditions based on Aydogdu model is an appropriate example. Ebrahimi and Barati [30] reported the wave propagation in nanoscales S-FGM beams embedded in elastic foundation subjected to longitudinal magnetic field by nonlocal strain gradient theory and the Euler–Bernoulli beam model.

At this juncture, it should be pointed out that the mid-surface and neutral surface in a homogeneous isotropic plate generally coincide whereas in the case of the FGM plate, they do not. The reason for the non- coincidence in the latter is that the elastic properties vary along the transverse direction. In the context of the FGM , many researchers (Yin et al. [31] ; Kim and Lee [32]; Lee et al. [33]; Zhang [34]; Zhang and Zhou [35]) employed the approach of the neutral surface variation in the constitutive equation of the FGM plate. As a consequence, they found that by selecting a proper reference plane, the coupling between the membrane and curvature modes can be eliminated. Furthermore, Abrate [36] took up the issue for the mechanics of functionally graded plates and elaborated on their tendency to act as a homogeneous and isotropic plate if the new reference plane is properly selected. In addition, Han et al. [37] carried out the dynamic instability analysis of sigmoid FGM plates considering physical neutral surface resting on Pasternak elastic foundations based on four-variable refined plate theory. On the other hand, Eltaher et al. [38] determined the physical neutral axis and obtained the eigenvalues of modified FG nanobeams on the basis of Euler–Bernoulli beam theory. They discussed the effects of the nonlocal parameter, elasticity ratio and density ratio on the eigenvalues of nanobeams**.** Zhang [39] presented the modelling of functionally graded beams based on higher order shear deformation theory (HSDT) and by properly accounting for the neutral surface. Ding et al. [40] discussed the geometrical nonlinear vibration analysis of FG Euler Bernoulli beam in tandem with neutral surface lying on the elastic foundation by using Von Kármán's plate theory.

In the current work, the computation of eigenvalues and eigenmodes for the natural vibration of the sigmoid functionally graded plates by an exact method known as the Dynamic Stiffness method (DSM) is proposed. The DSM is a powerful analytical method for free vibration analysis of structures and is well-known as a better alternate to the Finite Element Method [FEM]. The DSM has found wide applications and acceptance in recent years. It is based on exact shape functions, obtained from the exact solution of the governing differential equations. Hence, it is also called an exact method [41]. Since, the results from this method does not depend on the number of elements, it ensures much better accuracy and computational efficiency when compared with the finite element method (FEM) [42]. When dealing with high frequency vibration and when better accuracy is required, the use of the DSM is most effective. The basic building block in DSM is the frequency dependent dynamic stiffness matrix that comprises both mass and stiffness properties of individual elements. Unlike the FEM, there are no separate mass and stiffness matrices for each element in the DSM. FEM deals with linear eigenvalue problems whereas DSM deals with nonlinear eigenvalue problems. The elements of DSM are generally transcendental functions of the frequency and the application of Wittrick-Williams (W-W) algorithm as solution technique is extremely advantageous [43].

During our research, we carried out a detailed literature review and found that the papers published by Banerjee and his co-workers [44–48] and Ghorbel et al [49, 50] are probably the most notable contributions in recent years dealing with the free vibration characteristics of isotropic and orthotropic plates using DSM. Others researchers namely Boscolo and Banerjee [51–53]; Liu and Banerjee [54, 55]; Fazzolari et al. [56]; Thinh et al. [57] successfully employed the DSM with the application of the Wittrick-Williams algorithm to compute the eigenvalue and eigenvectors of the composite plates. Subsequent developments followed. For instance, Pagani et al.[58] formulated the DSM with the application of the Wittrick–Williams algorithm in computing the eigenvalue of composite beams subjected to different boundary conditions whereas Marjanović et al. [59] formulated the DSM for computing the eigenvalue of transversely isotropic multilayered rectangular plates subjected to different boundary conditions. The authors of [59] included the effects of various parameters such as face to core module ratio, face to core thickness ratio and shear deformation on the free vibration behaviour of sandwich plates. Employing a different approach in contrast to the previous ones, Kolarevic et al. [60] utilized the superposition technique and projection method to develop the DSM of rectangular plate assemblies. They used boundary layer function to change the three coupled Euler-Lagrange equations of motion into two uncoupled equations of motion. By contrast, Gupta and Talha [61] examined the influence of porosity on the flexural response of gradient plate using non-polynomial higher-order shear and normal deformation theory.

It is noted, after carefully going through the pertinent literature that various researchers have used various methods for computing the eigenvalue and eigenmodes of FGM plates, but to the best of the authors' knowledge, research leading to the analysis of free vibration characteristics of sigmoid functionally graded plate using the DSM has apparently not taken place, prior to the current one. Consequently, the novelty of the present work is the use of the DSM with the application of the Wittrick-Williams algorithm to determine the eigenvalues and eigenmodes of the sigmoid functionally graded plates. The results obtained from the DSM are compared with published results for some cases. The effects of different parameters of the S-FGM plate on its free vibration characteristics are discussed in detail. It is observed that the results obtained from DSM are highly accurate and can be used as a benchmark solution for further research on S-FGM plates.

The layout of the rest part of the paper are as follows: Following this section on introduction, section 2 describes the mathematical modelling for the sigmoid functionally graded plate considering the neutral surface. The formulation of DSM for a Levy type S- FGM plate based on Kirchhoff-Love plate theory is outlined in section 3. The assembly procedure for the DSM and application of the Wittrick–Williams algorithm are presented in section 4. Section 5 describes comparative study, parametric investigation and the effects of material properties on the frequency parameters of S-FGM plates. The conclusions of the investigation are presented in section 6.

2. Theory

2.1 Mathematical modelling for sigmoid functionally graded plate

In Fig. 1, an S-FGM plate which is an amalgamation of metal and ceramic is shown. The plate has a length L, width b and thickness h. The S-FGM plate comprises pure ceramic and pure metal on the upper and the lower surfaces, respectively. The material density $\rho(z_{ms})$ and Young's modulus $E(z_{ms})$ vary continuously and smoothly in the thickness direction by two power-law

functions (sigmoid law). Note that the suffices *ms* and *ns* in this paper indicate middle surface and neutral surface of the plate, respectively. Poisson's ratio is assumed to be constant because the influence of the Poisson's ratio (which has a value of around 0.3 and does not vary markedly in metal and ceramic) on the behaviour of the FGM plate seems to be much less signifant than that of the Young's modulus and density. Several researchers have employed the power law, exponential law and sigmoid law to define the volume fractions, but in the present study as already mentioned sigmoid law is used to define the volume fraction of the material.

The sigmoid law requirement is very important because due to this assumption the stress concentration more or less disappears at the interface of the materials of an S-FGM plate. The variation of volume fractions $V_f(z_{ms})$ of the constituents of the S-FGM plate through the thickness direction is given by two power law functions [21].

$$V_f{}^{(1)}(z_{ms}) = \frac{1}{2}\left(\frac{h/2+z_{ms}}{h/2}\right)^k \qquad for \qquad -h/2 \le z_{ms} \le 0$$
$$V_f{}^{(2)}(z_{ms}) = 1 - \frac{1}{2}\left(\frac{h/2-z_{ms}}{h/2}\right)^k \qquad for \qquad 0 \le z_{ms} \le h/2 \tag{1}$$

where k denotes the non-negative material gradient index that controls the volume fraction of the material in the thickness direction.

By using the rule of mixture, the material properties (P) are graded through the thickness direction according to the Voigt model as follows.

$$P_1(z_{ms}) = V_f{}^{(1)}(z_{ms})P_c + [1 - V_f{}^{(1)}(z_{ms})]P_m \qquad for \quad -h/2 \le z_{ms} \le 0$$
$$P_2(z_{ms}) = V_f{}^{(2)}(z_{ms})P_c + [1 - V_f{}^{(2)}(z_{ms})]P_m \qquad for \quad 0 \le z_{ms} \le h/2 \tag{2}$$

where $P_1(z_{ms})$ and $P_2(z_{ms})$ represents the typical material properties such as Young's modulus (E), material density (ρ) and Poisson's ratio (μ). P_c and P_m are the material properties of the ceramic and metal, respectively.

The Young's modulus and material density for the S-FGM plate vary along the transverse direction by the two power-law distribution function as shown in Fig. 2 (a) and (b), respectively.

2.2 Kirchoff- Love plate theory

According to Kirchoff- Love plate theory, the deformation field of an arbitrary point (x, y, z_{ms}) at any arbitrary time 't' can be expressed as [62]

$$u(x, y, z_{ms}, t) = u_0(x, y, t) - z_{ms}\varphi_y(x, y, t)$$
$$v(x, y, z_{ms}, t) = v_0(x, y, t) - z_{ms}\varphi_x(x, y, t) \tag{3}$$
$$w(x, y, z_{ms}, t) = w_0(x, y, t)$$

where, u, v, w are the displacement field of a point on the middle plane of the plate in the respective x, y, z direction, u_0 and v_0 are the membrane displacements and w_0 is the transverse displacement of a point on the middle plane, φ_x and φ_y are the bending rotations about the x and y axes, respectively.

The strain related to the above displacement field can be expressed as

$$\{\varepsilon\} = \begin{Bmatrix} \varepsilon_{xx} \\ \varepsilon_{yy} \\ \gamma_{xy} \end{Bmatrix} = \{\varepsilon^0{}_{xx}\} - z_{ms}\{k^0{}_{xx}\} \tag{4}$$

in which $\varepsilon^0{}_{xx}$ and $k^0{}_{xx}$ are the in-plane strains, and bending and twisting curvatures, respectively.

2.3 Neutral Surface

Unlike, homogeneous isotropic plates, the neutral surface of an S-FGM plate does not coincide with the mid surface of the plate. This is due to the variation of material properties along the thickness direction of the plate. Thus, neutral surface of an S-FGM plate will no longer be at the mid-surface. Figure 3 shows the position of neutral surface and middle surface for an S-FGM plate which are separated by a distance 'a'.

As the neutral surface takes a new coordinate system, its position can be defined as follows.

$$z_{ms} = z_{ns} + a \tag{5}$$

If the governing differential equation is based on the neutral surface, the S-FGM plate can be handled relatively easily because the coupling between the membrane and bending deformation in Kirchoff-Love plate theory will not be present.

The displacement fields which account for the position of the neutral surface are given below.

$$\begin{aligned} u &= -z_{ns}\frac{\partial w}{\partial x} = -(z_{ms} - a)\frac{\partial w}{\partial x} \\ v &= -z_{ns}\frac{\partial w}{\partial y} = -(z_{ms} - a)\frac{\partial w}{\partial y} \\ w &= w_0(x, y, t) \end{aligned} \tag{6}$$

The expressions for strain related to the above displacement field can be written as

$$\{\varepsilon\} = \begin{Bmatrix} \varepsilon_{xx} \\ \varepsilon_{yy} \\ \gamma_{xy} \end{Bmatrix} = -z_{ns}\begin{Bmatrix} \frac{\partial^2 w}{\partial x^2} \\ \frac{\partial^2 w}{\partial y^2} \\ 2\frac{\partial^2 w}{\partial xy} \end{Bmatrix} \tag{7}$$

In Eq. (7), ε_{xx} and ε_{yy} are normal strains and γ_{xy} is the shearing strain, respectively.

From the generalized Hooke's law, the stress is related to strain as

$$\sigma = [Q]\{\varepsilon\}$$

$$\begin{Bmatrix} \sigma_{xx} \\ \sigma_{yy} \\ \tau_{xy} \end{Bmatrix} = \begin{bmatrix} Q_{11} & Q_{12} & 0 \\ Q_{21} & Q_{22} & 0 \\ 0 & 0 & Q_{66} \end{bmatrix}\begin{Bmatrix} \varepsilon_{xx} \\ \varepsilon_{yy} \\ \gamma_{xy} \end{Bmatrix} \tag{8}$$

where σ_{xx}, σ_{yy} and τ_{xy} are the normal and shear stresses, respectively.

The elastic constants ($Q = Q_{ij}$) can be expressed as

$$Q_{ij} = \frac{E(z_{ns})}{1-\mu^2}\begin{bmatrix} 1 & \mu & 0 \\ \mu & 1 & 0 \\ 0 & 0 & \frac{1-\mu}{2} \end{bmatrix} \tag{9}$$

where (i, j =1, 2, 6) and μ is the Poisson's ratio already defined before.

The neutral surface is the surface in the cross-section of the plate where the material of the plate is not under any stress. The position of the neutral surface can be calculated by putting the total axial forces at the cross-section of the plate to zero, i.e

$$\sum F_x = \int_{-h/2-a}^{h/2-a} \sigma_{xx}\, dA = 0 \tag{10}$$

where $dA = b dz_{ns}$

Substituting Eq. (7) into Eq. (10) leads to

$$b \int_{-h/2-a}^{h/2-a} E(z_{ns}) z_{ns} \frac{\partial^2 w}{\partial x^2} d\, z_{ns} = 0 \tag{11}$$

where *b* is the width of the plate.

As the material properties vary along the transverse direction by two power-law functions, the above expression can be written as:

$$b\left[\int_{-h/2-a}^{0} E_1(z_{ns}) z_{ns} \frac{\partial^2 w}{\partial x^2} dz_{ns} + \int_{0}^{h/2-a} E_2(z_{ns}) z_{ns} \frac{\partial^2 w}{\partial x^2} dz_{ns}\right] = 0 \tag{12}$$

By varying the integration from z_{ns} to z_{ms}, Eq. (12) is written as

$$b\left[\int_{-h/2}^{0} E_1(z_{ms})(z_{ms} - a) \frac{\partial^2 w}{\partial x^2} dz_{ms} + \int_{0}^{h/2} E_2(z_{ms})(z_{ms} - a) \frac{\partial^2 w}{\partial x^2} dz_{ms}\right] = 0 \tag{13}$$

This implies,

$$b\left[\int_{-\frac{h}{2}}^{0} E_1(z_{ms}) z_{ms} dz_{ms} - a\int_{-\frac{h}{2}}^{0} E_1(z_{ms}) dz_{ms} + \int_{0}^{\frac{h}{2}} E_2(z_{ms}) z_{ms} dz_{ms} - a\int_{0}^{\frac{h}{2}} E_2(z_{ms}) dz_{ms}\right] = 0$$

Therefore, the location of neutral surface can be determined from the following equation

$$a = \frac{\int_{-h/2}^{0} E_1(z_{ms}) z_{ms} dz_{ms} + \int_{0}^{h/2} E_2(z_{ms}) z_{ms} dz_{ms}}{\int_{-h/2}^{0} E_1(z_{ms}) dz_{ms} + \int_{0}^{h/2} E_2(z_{ms}) dz_{ms}}$$

or,

$$a = \frac{\frac{h}{4}(E_c - E_m) + \frac{h(E_m - E_c)}{2(k+2)(k+1)}}{(E_c + E_m)} = \frac{h\left(\frac{1}{4}(E_{rat} - 1) + \frac{(1 - E_{rat})}{2(k+2)(k+1)}\right)}{(E_{rat} + 1)} \tag{14}$$

where

$$E_{rat} = E_c / E_m \tag{14a}$$

One can notice from the Eq. (14) that the nondimensional shift (*a/h*) of the S-FGM plate depends upon the value of Young's modulus ratio (E_c/E_m) and the material gradient index (*k*). The influence of the material gradient index (*k)* on the non-dimensional shift (*a/h*) for different

E_c/E_m is shown in Fig. 4. It is observed from Fig. 4 that when $E_c/E_m = 1$, the non-dimensional shift (*a/h*) is zero for the values of material gradient indices (*k* =0, 0.1, 0.2, 0.5, 1, 2, 5, 10, 20). This is due to the fact that, the neutral surface and mid surface of the plate coincide and subsequently, the plate behaves like a homogeneous isotropic plate. In addition, it is apparent from Fig. 4 that when $E_c/E_m \neq 1$, the non-dimensional shift increases significantly for values of $k< 2$ and becomes almost constant when *k* increases beyond the value of 2 (*i.e*. the value of non-dimensional shift (*a/h*) becomes an asymptotic curve as the value of *k* increases for a specific value of E_c/E_m). It is found that as the ratio E_c/E_m increases, the neutral surface of the S-FGM plate shifts from the mid-surface and approaches towards the upper surface which is rich in ceramic. This happens mainly because the ceramic constituent of the S-FGM plate has higher stiffness than the metallic constituent.

The material property functions and volume fractions $V_f(z_{ns})$ of the different types of FGM plates based on the neutral surface are shown in Table 1 [24].

Considering the shift in the neutral surface, the governing equation of motion and associated natural boundary conditions of the S-FGM plate are obtained using Hamilton's principle, as shown below.

Governing differential equation:

$$D^*\left(\frac{\partial^4 w_0}{\partial x^4} + 2\frac{\partial^4 w_0}{\partial x^2 \partial y^2} + \frac{\partial^4 w_0}{\partial y^4}\right) + I_0\frac{\partial^2 w_0}{\partial t^2} = 0 \tag{15}$$

Natural boundary conditions:

$$V_x = -D^*\left(\frac{\partial^3 w_0}{\partial x^3} + (2-\mu)\frac{\partial^3 w_0}{\partial x \partial y^2}\right)\delta w_0$$
$$M_{xx} = -D^*\left(\frac{\partial^2 w_0}{\partial x^2} + \mu\frac{\partial^2 w_0}{\partial y^2}\right)\delta\varphi_y \tag{16}$$

where V_x is the shear force (tranverse force), M_{xx} is the bending moment and D^* is the effective flexural rigidity, I_0 is inertial coefficients and μ is the Poisson's ratio for the S-FGM plate. The explicit expressions of $D^*$and I_0 used in Eq. (15) are given in Appendix A.

3. Formulation of the dynamic stiffness matrix for the S- FGM plate

The steps adopted in the formulation of the DSM for the S-FGM plate are as follows:

(*i*) The partial differential equation of motion (Eq. (15)) for the S- FGM plate is first solved by assuming harmonic oscillation, (*ii*) Next, generic boundary conditions are applied to the edges of the Levy-type S-FGM plate for both forces and displacements which are essentially the expressions of displacement, rotation, shear force and bending moment, (*iii*) Finally, the constants of integration are eliminated from the solution by establishing the relationship between the harmonically varying forces with those of the corresponding displacements to formulate the DSM.

The solution of Eq. (15) is sought in the traditional Levy form, i.e. the opposite edges of the plate are simply supported, which satisfies the boundary conditions in the following form:

$$w_0(x,y,t) = \sum_{m=1}^{\infty} W_m(x) e^{i\omega t} \sin(\alpha_m y) \tag{17}$$

where ω is the angular frequency, W_m is the amplitude of $w_0(x,y,t)$ and $\alpha_{m=} \frac{m\pi}{L}$

Obviously, m is the number of half sine waves in the x -direction with L being the length of the plate.

Substituting $w_0(x,y,t)$ from Eq. (17) into Eq. (15), the following ordinary differential equation is obtained:

$$\frac{d^4 W_m}{dx^4} - 2\alpha_m \frac{d^2 W_m}{dx^2} + \left(\alpha_m^4 - \frac{I_0 \omega^2}{D^*}\right) W_m = 0 \qquad m = 1,2,3 \ldots\ldots\ldots\ldots\ldots \infty \tag{18}$$

The four roots of the auxiliary or characteristic equation of Eq. (18) are determined on the basis of the nature of the roots and clearly two conditions are feasible:

Case 1. $\alpha_m^2 \geq \omega\sqrt{\frac{\rho h}{D^*}}$ All four roots are real $(r_{1m,}\ {-}r_{1m,}\ r_{2m,} - r_{2m})$

$$r_{1m} = \sqrt{\alpha_m^2 + \omega\sqrt{\frac{\rho h}{D^*}}}\ , \qquad r_{2m} = \sqrt{\alpha_m^2 - \omega\sqrt{\frac{\rho h}{D^*}}} \tag{19}$$

The solution is given by:

$$W_m(x) = A_m \cosh(r_{1m}x) + B_m \sinh(r_{1m}x) + C_m \cosh(r_{2m}x) + D_m \sinh(r_{2m}x) \tag{20}$$

Case 2. $\alpha_m^2 < \omega\sqrt{\frac{\rho h}{D^*}}$, Two roots are real and two roots are imaginary

$(r_{1m,}\ {-}r_{1m,}\ ir_{2m,} - i\, r_{2m})$

$$r_{1m} = \sqrt{\alpha_m^2 + \omega\sqrt{\frac{\rho h}{D^*}}}\ , \qquad r_{2m} = \sqrt{-\alpha_m^2 + \omega\sqrt{\frac{\rho h}{D^*}}} \tag{21}$$

The solution is given by:

$$W_m(x) = A_m \cosh(r_{1m}x) + B_m \sinh(r_{1m}x) + C_m \cos(r_{2m}x) + D_m \sin(r_{2m}x) \tag{22}$$

The formulation procedure of DSM for case 2 is shown below, but for case 1 it is not presented for the sake of brevity as it is followed in a similar manner.

The bending rotation (ϕ_y), shear force (V_x) and bending moment (M_{xx}) can be obtained from the known displacement w_0 (Eqs.(17) and (22)) with the help of the following expressions.

$$\phi_{ym}(x,y) = \varphi_{ym}(x)\sin(\alpha_m y) = -\{r_{1m}A_m \sinh(r_{1m}x) + r_{1m}B_m \cosh(r_{1m}x) - r_{2m}C_m \sin(r_{2m}x) + r_{2m}D_m \cos(r_{2m}x)\sin(\alpha_m y)\} \quad (23)$$

$$V_{xm}(x,y) = v_{xm}(x)\sin(\alpha_m y) = -D^*\{A_m\big({r_{1m}}^3 - (2-\mu){\alpha_m}^2 r_{1m}\big)\sinh(r_{1m}x) + B_m\,({r_{1m}}^3 - (2-\mu){\alpha_m}^2 r_{1m})\cosh(r_{1m}x) + C_m({r_{2m}}^3 + (2-\mu){\alpha_m}^2 r_{2m}\big)\sin(r_{2m}x) - D_m({r_{2m}}^3 + (2-\mu){\alpha_m}^2 r_{2m})\cos(r_{2m}x))\sin(\alpha_m y)\} \quad (24)$$

$$M_{xx_m}(x,y) = m_{xx_m}(x)\sin(\alpha_m y) = -D^*\{A_m({r_{1m}}^2 - \mu\,{\alpha_m}^2)\cosh(r_{1m}x) + B_m({r_{1m}}^2 - \mu\,{\alpha_m}^2)\sinh(r_{1m}x) - C_m({r_{2m}}^2 + \mu\,{\alpha_m}^2)\cos(r_{2m}x) - D_m({r_{1m}}^2 + \mu\,{\alpha_m}^2))\sin(r_{2m}x)\sin(\alpha_m y)\} \quad (25)$$

The generalized boundary conditions for displacements at both ends of the FGM plate as shown in Fig. 5 are:

$$\text{At} \quad \begin{matrix} x = 0 & W_m = W_a; & \varphi_{ym} = \varphi_{ya} \\ x = b & W_m = W_b; & \varphi_{ym} = \varphi_{yb} \end{matrix} \quad (26)$$

Similarly, generalized boundary conditions for forces at both ends of the FGM plate as shown in Fig. 5 are:

$$\text{At} \quad \begin{matrix} x = 0 & \upsilon_{xm} = -\upsilon_a; & m_{xx_m} = -m_a \\ x = b & \upsilon_{xm} = \upsilon_b; & m_{xx_m} = m_b \end{matrix} \quad (27)$$

By applying boundary conditions of Eq. (26) for displacement given by Eqs. (22) and (23), the following matrix relationship is obtained as.

$$\begin{bmatrix} W_a \\ \varphi_{y_a} \\ W_b \\ \varphi_{y_b} \end{bmatrix} = \begin{bmatrix} 1 & 0 & 1 & 0 \\ 0 & -r_{1m} & 0 & -r_{2m} \\ C_{h_1} & S_{h_1} & C_2 & S_2 \\ -r_{1m}S_{h_1} & -r_{1m}C_{h_1} & r_{2m}S_2 & -r_{2m}C_2 \end{bmatrix} \begin{bmatrix} A_m \\ B_m \\ C_m \\ D_m \end{bmatrix} \quad (28)$$

or,

$$\mathbf{X} = \mathbf{BC} \quad (29)$$

where

$$C_{h_1} = \cosh(r_{1m}b), \quad S_{h_1} = \sinh(r_{1m}b) \quad C_1 = \cos(r_{1m}b), \quad S_1 = \sin(r_{1m}b)$$
$$C_{h_2} = \cosh(r_{2m}b), \quad S_{h_2} = \sinh(r_{2m}b) \quad C_2 = \cos(r_{2m}b), \quad S_2 = \sin(r_{2m}b) \quad (30)$$

Similarly, by applying the boundary conditions of Eq. (27) for forces given by Eqs. (24) and (25), the following relationship matrix is obtained.

$$\begin{bmatrix} v_a \\ m_a \\ v_b \\ m_b \end{bmatrix} = \begin{bmatrix} 0 & R_1 & 0 & R_2 \\ L_1 & 0 & L_2 & 0 \\ -R_1 S_{h_1} & -R_1 C_{h_1} & R_2 S_{_2} & -R_2 C_{_2} \\ -L_1 C_{h_1} & -L_1 S_{h_1} & -L_2 C_{_2} & -L_2 S_{_2} \end{bmatrix} \begin{bmatrix} A_m \\ B_m \\ C_m \\ D_m \end{bmatrix}$$

or

$$\mathbf{F} = \mathbf{LC} \tag{31}$$

where

$$R_i = D^*(-1)^{i+1}\{r_{im}^3 - (2-\mu)\alpha^2 r_{im}\}; \qquad L_i = D^*(-1)^{i+1}(r_{im}^2 - \mu\alpha^2)$$

with $i = 1, 2$

The relationship between the forces and displacements can now be expressed as

$$\mathbf{F} = \mathbf{KX} \tag{32}$$

where $\mathbf{K}$ is the dynamic stiffness matrix given by

$$\mathbf{K} = \mathbf{LB^{-1}} \tag{33}$$

The six independent terms $s_{vv}, s_{vm}, f_{vv}, f_{vm}, s_{mm}, f_{mm}$ of the 4×4 symmetric dynamic stiffness form the fundamental basis of the analysis as expressed below.

$$\mathbf{K} = \begin{bmatrix} s_{vv} & s_{vm} & f_{vv} & f_{vm} \\ & s_{mm} & -f_{vm} & f_{mm} \\ & Sym & s_{vv} & -s_{vm} \\ & & & s_{mm} \end{bmatrix} \tag{34}$$

The explicit expressions for each of the terms of the dynamic stiffness matrix **K** are obtained by using symbolic algebra through the application of Matlab and they are given in Appendix B.

4. Assembly procedure for DSM

Plate structures may be subdivided into many elements or substructures for which each can be represented by the above DSM formulation. The elemental dynamic stiffness matrix (**K**) as expressed in Eq. (34) is the basic requirement to compute the exact eigenvalues of the S-FGM Levy-type plate. Therefore, global DSM for the S-FGM plate structure can be assembled directly from the assembly of several elements. A solution for natural frequencies to any desired accuracy can be achieved even by using a single DS element which of course, is not possible in FEM. Unlike the FEM, DS elements here do not have nodal points but have nodal lines at the interface. The assembly procedure for DSM of S-FGM plate is carried out in the same manner as it is performed in the FEM. The assembly procedure of the DSM is shown in Fig. 6. The overall global master matrix will always be a banded matrix as in the case of FEM [44].

4.1 Boundary conditions for S-FGM plate

The applications of boundary conditions to restrain any degrees of freedom in DSM are similar to that of FEM and usually the penalty method is employed. This method generally suppresses the degree of freedom (DOF) by attaching a very large stiffness to the appropriate term on the leading diagonal of the assembled dynamic stiffness matrix.

The following procedure is used to apply the boundary conditions.

- Free (F-F); no penalty is applied.
- Simply supported (S-S); transverse displacement (W) is penalized
- Clamped (C-C); transverse displacement (W) and bending rotation (φ_y) are penalized.

4.2 Application of the Wittrick –Williams algorithm

The Wittrick–Williams algorithm [43] is generally applied as solution technique for free vibration analysis of structures or structural elements using DSM. The global dynamic stiffness matrix of the plate structure contains the transcendental function of frequency for which the Wittrick–Williams algorithm is considered to be the best way to determine the natural frequencies without missing any. The algorithm takes into consideration the Sturm sequence property which guarantees that all naural frequencies are computed. The computational steps involved are shown in Fig. 7 using a flow chart.

5. Results and discussion

In order to compute the eigenvalues (natural frequencies) and eigenvectors (mode shapes) of S-FGM plates, a MATLAB program was developed using the above theory. In this section, results are presented and the significances of aspect ratio (L/b), material gradient index (k), boundary conditions and material properties on the eigenvalues of the S-FGM plate are discussed. Table 2 shows properties of the material constituents of the functionally graded plates reported by different researchers in the literature to investigate their free vibration characteristics. By and large, these properties [61] are used in obtaining the results of this paper.

The effect of different materials on the eigenvalue of the S-FGM plate is first demonstrated. The variations of fundamental natural frequency parameter defined in Eq. (35) below, with the material gradient index (k) are presented in Fig. 8 for different material constituents of the S-FGM plate. For lower value of k, for example, $k<2$, the natural frequency decreases for all the different materials used in the analysis. However, when k increases beyond the value of 2, the decrease in the natural frequency becomes less noticeable. It is also observed from the figure that there is significant reduction in the frequency parameter for Al /Al_2O_3 plate with increasing values of k, particularly in the range $0< k <5$. This is due to the large differences in the material properties of the constituent of the S-FGM plate, especially for the density. The figure also reveals the extent of the variation of the natural frequency of the plate depending upon the type of material used. The plates having lower values of Young's modulus (e.g. ZrO2/Ti-6Al-4V) being more flexible give lower values of natural frequencies, as expected.

5.1 Analysis of isotropic, FGM and S-FGM plates - a comparative study

In order to give a broad perspective and also for the purposes of comparison of results, various plate theories from the literature together with the proposed theory for the S-FGM plate are briefly outlined in Table 3 in order to set the scene and lead the readers smoothly to the subsequent text.

The natural frequency parameters for the isotropic, FGM and S-FGM plates used in the study are respectively defined in non-dimensional forms by ω^*, $\widehat{\omega}$, and $\overline{\omega}$ as follows.

$$\omega^* = \omega L^2 \sqrt{\frac{\rho h}{D^*}} \quad ; \qquad \widehat{\omega} = \omega \pi^2 \frac{L^2}{h} \sqrt{\frac{\rho_m}{E_m}} \quad ; \qquad \overline{\omega} = \omega \frac{L^2}{h} \sqrt{\frac{\rho_c}{E_c}} \tag{35}$$

where E_c and E_m are the modulus of elasticity and ρ_c and ρ_m are the material density of ceramic and metal of the S- FGM plate respectively.

First of all, attention is focused on the validation of results computed from the present theory. This is achieved by comparing the natural frequency parameters with the ones that are available in the literature for isotropic, FGM and S-FGM plates. A carefully selected samples of results to demonstrate the validation of results from different perspectives are given in Tables (4)-(8) for which the following material properties are used.

E_c=380 GPa; E_m = 69 GPa; ρ_c =3980 kg/m^3; $\rho_m = 2710$ kg/m^3.

Using standard notation, the number of half sine wave in the *x*-direction is represented by 'm' while the nth eigenvalue, for a certain value of m, is denoted by 'n' when presenting the results.

In the first example, see Tables 4 and 5, the natural frequency parameter (ω^*) for the first six natural frequencies of a rectangular isotropic plates for SSSS and SCSC boundary conditions computed by the present theory are compared with the published results of Boscolo and Banerjee [44] and Leissa [62]. The results are indeed in very good agreement as can be seen.

In the second example, seeTable 6, the frequency parameter ($\widehat{\omega}$) for the first five modes of a square FGM plate for SFSF boundary conditions computed by the present theory are compared with published results for different values of *k*. Clearly the eigenvalues from the present theory compare very well with those based on isogeometric analysis (IGA) using CPT with neutral surface reported by Yin et al [31] and the exact solution published by Beferani et al [63].

In the third example, see Table 7, the fundamental natural frequency parameter ($\widehat{\omega}_1$) of a rectangular FGM plate for simply supported (SSSS) boundary conditions computed by the present theory is compared with published results [31, 63] for different values of *k*. The results are in excellent agreement, as can be seen.

In the fourth example, see Table 8, the fundamental natural frequency parameter ($\bar{\omega}_1$) of a square S-FGM plate for SSSS boundary condition computed by the present theory is compared with published results [24, 64, 65, 66] for different values of *k* and length to thickness (*L/h*) ratio. The comparative results are those of Jung et al. [24], Hosseini-Hashemi et al. [64], Thai and Vo [65] and with Hosseini-Hashemi et al. [66] which are based on NTSDT, HSDT, SSDT, and, FSDT, respectively. The fundamental natural frequency computed by the present method agrees very well with published results, as can be seen in Table 8.

5.2 Analysis of S-FGM plates

Table 9 shows the first six natural frequency parameters ($\bar{\omega}$) of a rectangular Levy-type S-FGM plate based on the current theory with six common boundary conditions (SSSS, SFSS, SFSF, SFSC, SSSC and SCSC) for different values of *k*. Representative values of the aspect ratio *L/b* =2 and and thickness to length ratio *h/L*=0.01 are used in the data when obtaining the results.

It is clear from the results in Table 9 that with increasing values of *k*, the natural frequency parameter ($\bar{\omega}$) decreases for all of the boundary conditions. This is to be expected because the S- FGM plate has smaller ceramic constituents for higher values of *k* and hence its stiffness decreases. It is also observed that the natural frequency parameters ($\bar{\omega}$) of the S-FGM plat are highest for SCSC boundary condition and lowest for SFSF boundary condition for a given value of *k*. This is because, as the constraints on the edges of the plate increases, the stiffness of the plate increases which leads to an increase in the natural frequency parameter ($\bar{\omega}$).

Four representive mode shapes of an S-FGM square plate subjected to SSSS and SSSF boundary conditions for *h/L*=0.01, *k*=0.5 are presented in Figs. 9 and 10, respectively. They follow more or less similar trends as observed in isotropic plates, but of course, the natural frequency can be markedly different.

5.3 A parametric investigation

In the next stage of the investigation, a parametric study was carried out to examine the effects of different parameters such as the aspect ratio (*L/b)*, material gradient index (*k)*, Young's modulus ratio (E_c/E_m) and the density ratio (ρ_c/ρ_m)) on the frequency parameter of the S-FGM plate.

Figures 11(a) and 11(b) illustrate the variations of the fundamental natural frequency parameter ($\bar{\omega}_1$) with respect to the change in the aspect ratio (*L/b*) for different values of *k* for SCSC and SFSF boundary conditions, respectively. Fig. 11(a) shows that with the increase in the aspect ratio (*L/b*), the fundamental natural frequency parameter ($\bar{\omega}_1$) increases for all values of *k*. For isotropic and homogeneous plates (i.e. when $k = 0$ in the current theory), similar observation was made by Leissa, see his result in Table A2 of [62]. A similar trend for the variation of ($\bar{\omega}_1$) is observed for all other boundary conditions (which are not presented here for brevity) except for the SFSF case which is shown in Fig. 11 (b) . The fundamental natural frequency parameter ($\bar{\omega}_1$) of the plate under SFSF boundary conditions decreases with the increase in the aspect ratio. This trend is same as that was found in isotropic homogeneous plates, see Table A6 of [62].

In order to ascertain the effect of different boundary conditions on the fundamental natural frequency parameter ($\bar{\omega}_1$) of the rectangular S- FGM plate, the variations of the fundamental natural frequency parameter ($\bar{\omega}_1$) with aspect ratio (*L/b*) under different boundary conditions are shown in Fig. 12. The figure shows that fundamental natural frequency parameter ($\bar{\omega}_1$) increases as the aspect ratio (*L/b*) increases for all five boundary conditions, except for the SFSF boundary condition. This is in accord with the analysis carried out by Leissa [62] for isotropic homogeneous plates. Furthermore, it is revealed in Fig. 12 that the change of the fundamental natural frequency parameter ($\bar{\omega}_1$) for the SCSC boundary condition is the highest and under SFSF it is the lowest for a given (*L/b*) value. The fundamental natural frequency parameter ($\bar{\omega}_1$) of SCSC boundary condition has the highest value, and SFSF has the lowest value compared to the other boundary conditions considered in the analysis, as expected [62].

Figures 13 (a) and (b) illustrate the variations that occur in the fundamental natural frequency parameter ($\bar{\omega}_1$) of an S-FGM plate for the SSSS and SFSF boundary conditions, respectively due to the change in the material gradient index (*k*) for different values of the aspect ratio *L/b*. The figures show the trend in which the fundamental natural frequency parameter ($\bar{\omega}_1$) decreases with the increase in the values of *k* for any specific value of the aspect ratio *L/b*. It is also observed from the figures that there is a substantial decrease in the fundamental natural frequency parameter ($\bar{\omega}_1$) as the values of *k* approaches to 0.5, but the decrease in the fundamental natural frequency parameter ($\bar{\omega}_1$) is not so pronounced when the values of *k* increases further. The same trends were observed for the boundary conditions vis-à-vis SFSS, SFSC, SSSC, and SCSC which are not shown here for brevity.

5.4 Effect of material properties

The influence of the material properties, namely the material density (ρ) and the Young's modulus (E) on the natural frequency parameter ($\bar{\omega}$) for the S-FGM plate is presented and discussed in this section. Using the variations in the Young's modulus ratio (E_c/E_m), while keeping material density ratio constant (i.e. $\rho_c/\rho_m = 1$) brings about subsequent variations in the natural frequency parameter ($\bar{\omega}$) of the square S- FGM plate which is illustrated in Fig. 14 for the first six modes of vibration for SCSS boundary condition. Additionally, it is noticed that with an increase in the Young's modulus ratio (E_c/E_m), the frequency parameter ($\bar{\omega}$), in general, decreases. However, this decrease in natural frequency is significant for lower values of the Young's modulus ratio, particularly when (E_c/E_m) < 5. The validity of this statement can be established by using Eq. (35), which factors in the condition that ($\bar{\omega}$) is inversely proportional to the Young's modulus of the ceramic materials of the S-FGM plate.

Figure 15 highligths the variations in the natural frequency parameter ($\bar{\omega}$) due to the change in the material density ratio (ρ_c/ρ_m) while keeping the Young's modulus ratio constant (E_c/E_m =1) for the first six modes of vibration for SCSS boundary condition. An interpretation of the figure reveals that an increase in the frequency parameter ($\bar{\omega}$) is affected by an increase in the material density ratio (ρ_c/ρ_m). The validity of this statement can be established by using Eq. (35), which is due to the condition that ($\bar{\omega}$) is directly proportional to the material density of the ceramic materials of the S-FGM plate.

Figures 16 and 17, illustrate two different cases for the variations of material properties ratio, namely material density and Young's modulus ratio of the S-FGM plate on the fundamental natural frequency parameter ($\bar{\omega}_1$) for different values of *k* for the SCSS boundary condition. In the first case (Fig. 16), $\rho_c/\rho_m$is kept constant (i.e. $\rho_c/\rho_m = 1$), but E_c/E_m is varied between 1 and 40 and the corresponding effects on the fundamental natural frequency parameter ($\bar{\omega}_1$) are presented. Simultaneously, it is also noted that with an increase in E_c/E_m, there is a decrease in the fundamental natural frequency parameter ($\bar{\omega}_1$). Moreover, from the figure, it is noted that the fundamental natural frequency parameter ($\bar{\omega}_1$) decreases quite drastically when the value of E_c/E_m lies between 1 and 10. However, when E_c/E_m increases beyond 10, there is much less decrease in the fundamental natural frequency parameter ($\bar{\omega}_1$).

In the second case (Fig. 17), both the Young's modulus ratio and the density ratio are assumed to be the same, i.e. $E_c/E_m = \rho_c/\rho_m$ which varies from 1 to 40 and the corresponding effects on the fundamental natural frequency parameter ($\bar{\omega}_1$) for the SCSS boundary condition are

highlighted. The figure depicts the trend in which the fundamental natural frequency parameter ($\bar{\omega}_1$) decreases as the $E_c/E_m = \rho_c/\rho_m$ ratio increases. At this juncture, it must be noted that a substantial decrease in the fundamental natural frequency parameter ($\bar{\omega}_1$) is apparent for $E_c/E_m = \rho_c/\rho_m$<10 whereas less decrease is noted in the fundamental natural frequency parameter ($\bar{\omega}_1$) beyond this value, particularly for lower value of material gradient index (k).

The variations of the fundamental natural frequency parameter ($\bar{\omega}_1$) of the square S- FGM plate with ρ_c/ρ_m for different Young's modulus ratio (i.e. E_{rat}= 1, 2, 5, 10, 20, 40) for SCSS and SFSF boundary conditions are shown in Figs. 18 and 19, respectively.

An inspection of the Figs. 18 and 19, highlights the fact that an increase in the values of ρ_c/ρ_m results in the increase of the fundamental natural frequency parameter ($\bar{\omega}_1$). It is also noted that the fundamental natural frequency parameter ($\bar{\omega}_1$) increases significantly in the range of $1 \leq \rho_c/\rho_m \leq 10$. However, the increase in the fundamental natural frequency parameter ($\bar{\omega}_1$) is not so significant when ρ_c/ρ_m increases beyond 10.

6. Conclusions

The dynamic stiffness method (DSM) is developed for the investigation of natural vibration characteristics of sigmoid FGM Levy type plate considering physical neutral surface. The DSM is proved to be efficient and accurate when computing the eigenvalue of both isotropic and S-FGM plate structures. The eigenvalues obtained by the DSM with the application of the Wittrick-Williams algorithm match very well with published results. A comprehensive set of results is presented. The results obtained by the present method for isotropic and FGM plates when compared with published results in the literature revealed excellent agreement. The accuracy of the present method is verified through the study of natural vibration of S-FGM plates. The influences of various plate parameters such as material gradient index, aspect ratio, boundary conditions and material properties on the eigenvalues of S-FGM plate are analyzed and discussed in detail. For all modes and aspect ratios, the eigenvalues decrease as the values of the material gradient index of the S- FGM plate increase. The influence of the material gradient index on the fundamental frequency is substantial for the lower value of the material gradient index. The eigenvalues increase with an increase in the aspect ratio of the plate. The eigenvalue decreases when constraints change from the clamped edge condition to free edge condition because of the decrease in stiffness. It is interesting to note that with the increase in the E_c/E_m ratio, the fundamental frequency parameter decreases but the trends are reversed with an

increment in ρ_c/ρ_m. The variations of E_c/E_m and ρ_c/ρ_m substantially affect the natural frequency and cannot be disregarded. The main contribution made in this paper is of course, the development of the DSM for S-FGM plates in order to provide highly accurate results for their eigenvalues and mode shapes. The results obtained can be used as benchmark solution to validate FEM and other approximate methods.

Appendix A

Explicit expressions for D^* and I_0 in equations (15) and (16)

$$I_0 = \int_{-h/2-a}^{h/2-a} \rho(z_{ns}) dz_{ns}$$

$$= \int_{-h/2-a}^{0} \rho_1(z_{ns}) dz_{ns} + \int_{0}^{h/2-a} \rho_2(z_{ns}) dz_{ns}$$

$$= \int_{-h/2}^{0} \rho_1(z_{ms}) dz_{ms} + \int_{0}^{h/2} \rho_2(z_{ms}) dz_{ms}$$

$$= 0.5h\rho_c \left(1 + \frac{1}{\rho_{rat}}\right)$$

where

$$\rho_{rat} = \frac{\rho_c}{\rho_m}$$

$$D^* = \int_{-h/2-a}^{h/2-a} z_{ns}^2 \, Q_{11}(z_{ns}) dz_{ns} = \int_{-h/2-a}^{0} z_{ns}^2 \, Q_{11}(z_{ns}) dz_{ns} + \int_{0}^{h/2-a} z_{ns}^2 Q_{11}(z_{ns}) dz_{ns}$$

$$= \int_{-h/2}^{0} (z_{ms} - a)^2 Q_{11}(z_{ms}) dz_{ms} + \int_{0}^{h/2} (z_{ms} - a)^2 Q_{11}(z_{ms}) dz_{ms}$$

$$= 12(D_c/E_{rat})\left(0.5 \frac{a}{h}(1 - E_{rat})\left(\frac{1}{k+2} - \frac{1}{k+1}\right) + \frac{1}{24}(1 + E_{rat}) + 0.5 \left(\frac{a}{h}\right)^2 (1 + E_{rat}) + 0.25 \frac{a}{h} (1 - E_{rat})\right)$$

where

$D_c = \frac{E_c h^3}{12(1-\mu^2)}$ is the flexural rigidity of the ceramic material and $E_{rat} = \frac{E_c}{E_m}$

Appendix B

Explicit expressions for the dynamic stiffness elements of equation (34)

$$s_{mm} = (L_1 - L_2)(r_{1m}C_{h_1}S_2 - r_{2m}C_2S_{h_1})/\nabla,$$
$$s_{vv} = (r_{2m}R_1 + r_{1m}R_2)(r_{2m}C_{h_1}S_2 + r_{1m}C_2S_{h_1})/\nabla,$$
$$s_{vm} = -(r_{2m}(R_1\left({C_2}^2 - C_2C_{h_1} + {S_2}^2\right) - R_2S_2S_{h_1}) - r_{1m}(R_1S_2S_{h_1} - R_2((C_2 - C_{h_1})C_{h_1} + {S_{h_1}}^2))/\nabla,$$
$$f_{mm} = (L_2 - L_1)(r_{1m}S_2 - r_{2m}S_{h_1})/\nabla,$$
$$f_{vv} = (r_{1m}R_2 - r_{2m}R_1)(r_{2m}S_2 + r_{1m}S_{h_1})/\nabla,$$
$$f_{vm} = (C_2 - C_{h_1})(r_{2m}R_1 - r_{1m}R_2)/\nabla,$$

where

$$R_i = D^*(-1)^{i+1}\left(r_{im}^3 - (2-\mu)\alpha^2 r_{im}\right); \qquad L_i = D^*(-1)^{i+1}(r_{im}^2 - \mu\alpha^2) \qquad i = 1,2$$

$$C_{h_1} = \cosh(r_{1m}b), \qquad S_{h_1} = \sinh(r_{1m}b) \qquad C_1 = \cos(r_{1m}b), \qquad S_1 = \sin(r_{1m}b)$$

$$C_{h_2} = \cosh(r_{2m}b), \qquad S_{h_2} = \sinh(r_{2m}b) \qquad C_2 = \cos(r_{2m}b), \qquad S_2 = \sin(r_{2m}b)$$

and

$$\nabla = {r^2}_{1m}S_2S_{h_1} - {r^2}_{2m}S_2S_{h_1} + r_{1m}r_{2m}\left((C_2 - C_{h_1})^2 + {S_2}^2 - {S_{h_1}}^2\right)$$

References

[1] L.F. Qian, R.C. Batra, Design of bidirectional functionally graded plate for optimal natural frequencies, J. Sound Vib. 280 (2005) 415–424. doi:10.1016/j.jsv.2004.01.042.

[2] D.Y. Liu, C.Y. Wang, W.Q. Chen, Free vibration of FGM plates with in-plane material inhomogeneity, Compos. Struct. 92 (2010) 1047–1051 doi:10.1016/j.compstruct.2009 .10.001.

[3] M. Koizumi, FGM activities in Japan, Compos. Part B Eng. 28 (1997) 1–4. doi:https ://doi.org/10.1016/S1359-8368(96)00016-9.

[4] S. Suresh, A. Mortensen, Functionally graded metals and metal-ceramic composites: Part 2 Thermomechanical behaviour, Int. Mater. Rev. 42 (1997) 85–116. doi:10.1179 / imr.1997.42.3.85.

[5] V. Birman, L.W. Byrd, Modeling and analysis of functionally graded materials and structures, Appl. Mech. Rev. 60 (2007) 195-216. doi:10.1115/1.2777164.

[6] S. Suresh, A. Mortensen, Fundamentals of functionally graded materials, Mater. Today. 1 (1998) 18. doi:10.1016/s1369-7021(98)80023-0.

[7] I. Shiota, Y. Miyamoto, Functionally graded materials, in: Proc. 4th Int. Symp. Funct. Graded Mater., Elseveir, AIST Tsukuba Research center, Tsukuba, Japan, (1996) 1– 803.

[8] Z.-H. Jin, G.H. Paulino, Transient thermal stress analysis of an edge crack in a functionally graded material, Int. J. Fract. 107 (2001) 73–98. doi:10.1023/ A:1026583903046.

[9] Y.Y. Yang, D. Munz, Stress analysis in a two materials joint with a functionally graded material, Proc. 4th Int. Symp. Funct. Graded Mater. (1997) 41–46. doi:10.1016/ B978-044482548-3/50008-1.

[10] M. Talha, B.N. Singh, Static response and free vibration analysis of FGM plates using higher order shear deformation theory, Appl. Math. Model. 34 (2010) 3991–4011. doi:10.1016/j.apm.2010.03.034.

[11] B. Uymaz, M. Aydogdu, S. Filiz, Vibration analyses of FGM plates with in-plane material inhomogeneity by Ritz method, Compos. Struct. 94 (2012) 1398–1405. doi:10.1016/j.compstruct.2011.11.002.

[12] H. Ait Atmane, A. Tounsi, I. Mechab, E.A. Adda Bedia, Free vibration analysis of functionally graded plates resting on Winkler–Pasternak elastic foundations using a new shear deformation theory, Int. J. Mech. Mater. Des. 6 (2010) 113–121. doi:10.1007/s10999-010-9110-x.

[13] X. Zhao, Y.Y. Lee, K.M. Liew, Free vibration analysis of functionally graded plates using the element-free kp-Ritz method, J. Sound Vib. 319 (2009) 918–939. doi:10.1016/j.jsv.2008.06.025.

[14] A.M.A. Neves, A.J.M. Ferreira, E. Carrera, M. Cinefra, C.M.C. Roque, R.M.N. Jorge, C.M.M. Soares, A quasi-3D hyperbolic shear deformation theory for the static and free vibration analysis of functionally graded plates, Compos. Struct. 94 (2012) 1814–1825. doi:10.1016/j.compstruct.2011.12.005.

[15] Z. Jin, R.C. Batra, Stress intensity relaxation at the tip of an edge crack in a functionally graded material subjected to a thermal shock, J. Therm. Stress. 19 (1996) 317–339. doi:10.1080/01495739608946178.

[16] F. Delale, F. Erdogan, The crack problem for a nonhomogeneous plane, J. Appl. Mech. 50 (1983) 609–614. doi: 10.1115/1.3167098

[17] P. Gu, R.J. Asaro, Crack deflection in functionally graded materials, Int. J. Solids Struct. 34 (1997) 3085–3098. doi:10.1016/S0020-7683(96)00175-8.

[18] F. Erdogan, B.H. Wu, Crack problems in fgm layers under thermal stresses, J. Therm. Stress. 19 (1996) 237–265. doi:10.1080/01495739608946172.

[19] Z. Jin, N. Noda, Crack-tip singular fields in nonhomogeneous materials, J. Appl. Mech. 39 (1994) 1987–1989. doi:10.1115/1.2901529.

[20] Y.F. Erdogan, F. Chen, Interfacial cracking of FGM metal bonds, In: Kokini, K. (Ed.), Ceramic Coating. (1998) 29–37..

[21] Y.-L. Chung, S.H. Chi, The residual stress of functionally graded materials, J. Chinese Inst. Civil hydr. Eng. 13 (2001) 1-9.

[22] S.H. Chi, Y.-L. Chung, Cracking in sigmoid functionally graded coating, J. Mech. 18 (2002) 41–53.

[23] S.H. Chi, Y.L. Chung, Mechanical behavior of functionally graded material plates under transverse load-Part I: Analysis, Int. J. Solids Struct. 43 (2006) 3657–3674. doi:10.1016/j.ijsolstr.2005.04.011.

[24] W.Y. Jung, S.C. Han, W.T. Park, Four-variable refined plate theory for forced-vibration analysis of sigmoid functionally graded plates on elastic foundation, Int. J. Mech. Sci. 111–112 (2016) 73-87. doi:10.1016/j.ijmecsci.2016.03.001.

[25] F.A. Fazzolari, Modal characteristics of P- and S-FGM plates with temperature-dependent materials in thermal environment, J. Therm. Stress. 39 (2016) 854–873. doi:10.1080/01495739.2016.1189772.

[26] W.Y. Jung, W.T. Park, S.C. Han, Bending and vibration analysis of S-FGM microplates embedded in Pasternak elastic medium using the modified couple stress theory, Int. J. Mech. Sci. 87 (2014) 150–162. doi:10.1016/j.ijmecsci.2014.05.025.

[27] Y.Q. Wang, J.W. Zu, Large-amplitude vibration of sigmoid functionally graded thin plates with porosities, Thin-Walled Struct. 119 (2017) 911–924. doi:https://doi.org/10.1016/j.tws.2017.08.012.

[28] Y.Q. Wang, J.W. Zu, Vibration characteristics of moving sigmoid functionally graded plates containing porosities, Int. J. Mech. Mater. Des. 14 (2018) 473–489. doi:10.1007/s10999-017-9385-2.

[29] S. Ben-Oumrane, T. Abedlouahed, M. Ismail, B.B. Mohamed, M. Mustapha, A.B. El Abbas, A theoretical analysis of flexional bending of Al/Al2O3 S-FGM thick beams, Comput. Mater. Sci. 44 (2009) 1344–1350. doi:10.1016/j.commatsci.2008.09.001.

[30] F. Ebrahimi, M.R. Barati, Flexural wave propagation analysis of embedded S-FGM nanobeams under longitudinal magnetic field based on nonlocal strain gradient theory, Arab. J. Sci. Eng. 42 (2017) 1715–1726. doi:10.1007/s13369-016-2266-4.

[31] S. Yin, T. Yu, P. Liu, Free vibration analyses of FGM thin plates by isogeometric analysis based on classical plate theory and physical neutral surface, Adv. Mech. Eng. 5 (2013) 1-10. doi:10.1155/2013/634584.

[32] N. Il Kim, J. Lee, Geometrically nonlinear isogeometric analysis of functionally graded plates based on first-order shear deformation theory considering physical neutral surface, Compos. Struct. 153 (2016) 804–814. doi:10.1016/j.compstruct.2016.07.002.

[33] Y.H. Lee, S.I. Bae, J.H. Kim, Thermal buckling behavior of functionally graded plates based on neutral surface, Compos. Struct. 137 (2016) 208–214. doi:10.1016/j.compstruct.2015.11.023.

[34] D.G. Zhang, Nonlinear bending analysis of FGM beams based on physical neutral surface and high order shear deformation theory, Compos. Struct. 100 (2013) 121–126. doi:10.1016/j.compstruct.2012.12.024.

[35] D.G. Zhang, Y.H. Zhou, A theoretical analysis of FGM thin plates based on physical neutral surface, Comput. Mater. Sci. 44 (2008) 716–720. doi:10.1016/j.commatsci.2008.05.016.

[36] S. Abrate, Functionally graded plates behave like homogeneous plates, Compos. Part B Eng. 39 (2008) 151–158. doi:10.1016/j.compositesb.2007.02.026.

[37] S.C. Han, W.T. Park, W.Y. Jung, A four-variable refined plate theory for dynamic stability analysis of S-FGM plates based on physical neutral surface, Compos. Struct. 131 (2015) 1081–1089. doi:10.1016/j.compstruct.2015.06.025.

[38] M.A. Eltaher, A.E. Alshorbagy, F.F. Mahmoud, Determination of neutral axis position and its effect on natural frequencies of functionally graded macro/nanobeams, Compos. Struct. 99 (2013) 193–201. doi:10.1016/j.compstruct.2012.11.039.

[39] D.G. Zhang, Modeling and analysis of FGM rectangular plates based on physical neutral surface and high order shear deformation theory, Int. J. Mech. Sci. 68 (2013) 92–104. doi:10.1016/j.ijmecsci.2013.01.002.

[40] J. Ding, L. Chu, L. Xin, G. Dui, Nonlinear vibration analysis of functionally graded beams considering the influences of the rotary inertia of the cross section and neutral surface position, Mech. Based Des. Struct. Mach. 46 (2018) 225–237. doi:10.1080/15397734.2017.1329020.

[41] J.R. Banerjee, Dynamic stiffness formulation for structural elements: A general approach, Comput. Struct. 63 (1997) 101–103. doi:10.1016/S0045-7949(96)00326-4.

[42] A.Y.T. Leung, Dynamic Stiffness and Substructures, Springer-Verlag, London, 1993.

[43] W.H. Wittrick, F.W. Williams, A general algorithm for computing natural frequencies of elastic structures, Q. J. Mech. Appl. Math. XXIV (1971) 263–284. doi.org/10.1093/qjmam/24.3.263

[44] M. Boscolo, J.R. Banerjee, Dynamic stiffness elements and their applications for plates using first order shear deformation theory, Comput. Struct. 89 (2011) 395–410. doi:10.1016/j.compstruc.2010.11.005.

[45] M. Boscolo, J.R. Banerjee, Dynamic stiffness method for exact inplane free vibration analysis of plates and plate assemblies, J. Sound Vib. 330 (2011) 2928–2936. doi:10.1016/j.jsv.2010.12.022.

[46] S. Papkov, J.R. Banerjee, A new method for free vibration and buckling analysis of rectangular orthotropic plates, J. Sound Vib. 339 (2015): 342-358. doi:10.1016/j.jsv.2014.11.007.

[47] J.R. Banerjee, S.O. Papkov, X. Liu, D. Kennedy, Dynamic stiffness matrix of a rectangular plate for the general case, J. Sound Vib. 342 (2015) 177–199. doi:https://doi.org/10.1016/j.jsv.2014.12.031.

[48] X. Liu, J.R. Banerjee, Free vibration analysis for plates with arbitrary boundary conditions using a novel spectral-dynamic stiffness method, Comput. Struct. 164 (2016) 108–126. doi:https://doi.org/10.1016/j.compstruc.2015.11.005.

[49] O. Ghorbel, J.B. Casimir, L. Hammami, I. Tawfiq, M. Haddar, Dynamic stiffness formulation for free orthotropic plates, J. Sound Vib. 346 (2015) 361–375. doi:https://doi.org/10.1016/j.jsv.2015.02.020.

[50] O. Ghorbel, J.B. Casimir, L. Hammami, I. Tawfiq, M. Haddar, In-plane dynamic stiffness matrix for a free orthotropic plate, J. Sound Vib. 364 (2016) 234–246. doi:https://doi.org/10.1016/j.jsv.2015.11.028.

[51] M. Boscolo, J.R. Banerjee, Dynamic stiffness formulation for composite Mindlin plates for exact modal analysis of structures. Part I: Theory, Comput. Struct. 96 (2012) 61-73. doi:10.1016/j.compstruc.2012.01.002.

[52] M. Boscolo, J.R. Banerjee, Dynamic stiffness formulation for composite Mindlin plates for exact modal analysis of structures. Part II: Results and applications, Comput. Struct. 96 (2012) 74–83. doi:https://doi.org/10.1016/j.compstruc.2012.01.003.

[53] M. Boscolo, J.R. Banerjee, Layer-wise dynamic stiffness solution for free vibration analysis of laminated composite plates, J. Sound Vib. 333 (2014) 200–227. doi:10.1016/j.jsv.2013.08.031.

[54] X. Liu, J.R. Banerjee, An exact spectral-dynamic stiffness method for free flexural vibration analysis of orthotropic composite plate assemblies – Part I: Theory, Compos. Struct. 132 (2015) 1274–1287. doi:https://doi.org/10.1016/j.compstruct.2015.07.020.

[55] X. Liu, J.R. Banerjee, An exact spectral-dynamic stiffness method for free flexural vibration analysis of orthotropic composite plate assemblies – Part II: Applications, Compos. Struct. 132 (2015) 1288–1302. doi:https://doi.org/10.1016/j.compstruct.2015.07.022.

[56] F.A. Fazzolari, M. Boscolo, J.R. Banerjee, An exact dynamic stiffness element using a higher order shear deformation theory for free vibration analysis of composite plate assemblies, Compos. Struct. 96 (2013) 262–278. doi:10.1016/j.compstruct.2012.08.033.

[57] T.I. Thinh, M.C. Nguyen, D.G. Ninh, Dynamic stiffness formulation for vibration analysis of thick composite plates resting on non-homogenous foundations, Compos. Struct. 108 (2014) 684–695. doi:10.1016/j.compstruct.2013.10.022.

[58] A. Pagani, E. Carrera, M. Boscolo, J.R. Banerjee, Refined dynamic stiffness elements applied to free vibration analysis of generally laminated composite beams with arbitrary boundary conditions, Compos. Struct. 110 (2014) 305–316. doi:10.1016/j.compstruct.2013.12.010.

[59] M. Marjanović, N. Kolarević, M. Nefovska-Danilović, M. Petronijević, Free vibration study of sandwich plates using a family of novel shear deformable dynamic stiffness elements: limitations and comparison with the finite element solutions, Thin-Walled Struct. 107 (2016) 678–694. doi:10.1016/j.tws.2016.08.002.

[60] N. Kolarevic, M. Marjanović, M. Nefovska-Danilovic, M. Petronijevic, Free vibration analysis of plate assemblies using the dynamic stiffness method based on the higher order shear deformation theory, J. Sound Vib. 364 (2016) 110–132. doi:10.1016/j.jsv.2015.11.016.

[61] A. Gupta, M. Talha, Influence of porosity on the flexural and vibration response of gradient plate using nonpolynomial higher-order shear and normal deformation theory, Int. J. Mech. Mater. Des. 14 (2018) 277–296. doi:10.1007/s10999-017-9369-2.

[62] A.W. Leissa, the Free Vibration Of rectangular Plates, J. Sound Vib. 31 (1973) 257–293. doi:10.1016/S0022-460X(73)80371-2.

[63] A. Hasani Baferani, A.R. Saidi, E. Jomehzadeh, An exact solution for free vibration of thin functionally graded rectangular plates, Proc. Inst. Mech. Eng. Part C J. Mech. Eng. Sci. 225 (2011) 526–536. doi:10.1243/09544062JMES2171.

[64] S. Hosseini-Hashemi, M. Fadaee, S.R. Atashipour, Study on the free vibration of thick functionally graded rectangular plates according to a new exact closed-form procedure, Compos.Struct.93(2011)722–735.doi:https://doi.org/10.1016/j.compstruct. 2010.08.007.

[65] H.-T. Thai, T.P. Vo, A new sinusoidal shear deformation theory for bending, buckling, and vibration of functionally graded plates, Appl. Math. Model. 37 (2013) 3269–3281. doi:https://doi.org/10.1016/j.apm.2012.08.008.

[66] S. Hosseini-Hashemi, M. Fadaee, A. S.R, A new exact analytical approach for free vibration of Reissner–Mindlin functionally graded rectangular plates, Int. J. Mech. Sci. 53 (2011) 11-22. doi:10.1016/j.ijmecsci.2010.10.002.

Declaration of interests

☒ The authors declare that they have no known competing financial interests or personal relationships that could have appeared to influence the work reported in this paper.

☐The authors declare the following financial interests/personal relationships which may be considered as potential competing interests:

Figure

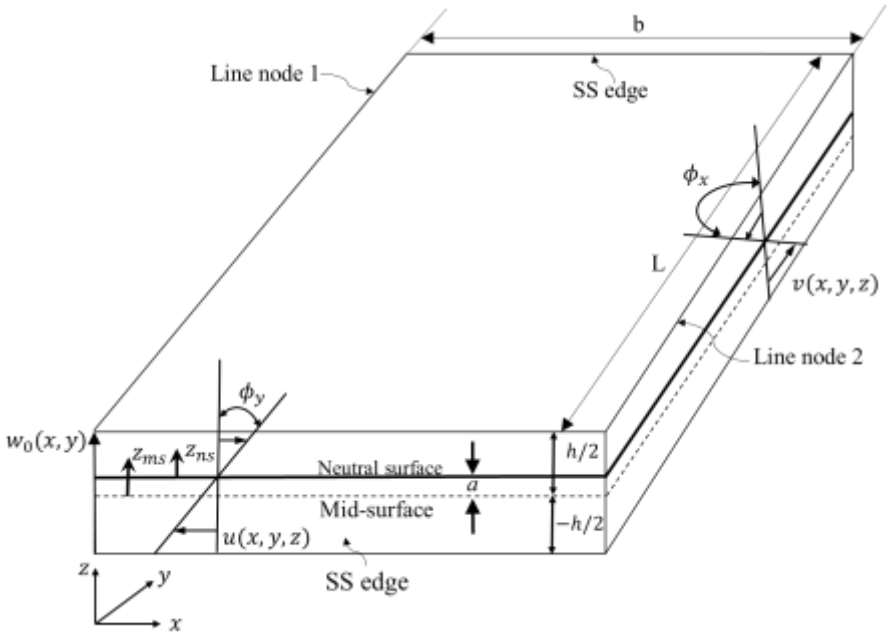

Fig. 1. Co-ordinate system and notation for the deformation field of an S- FGM plate.

Figure

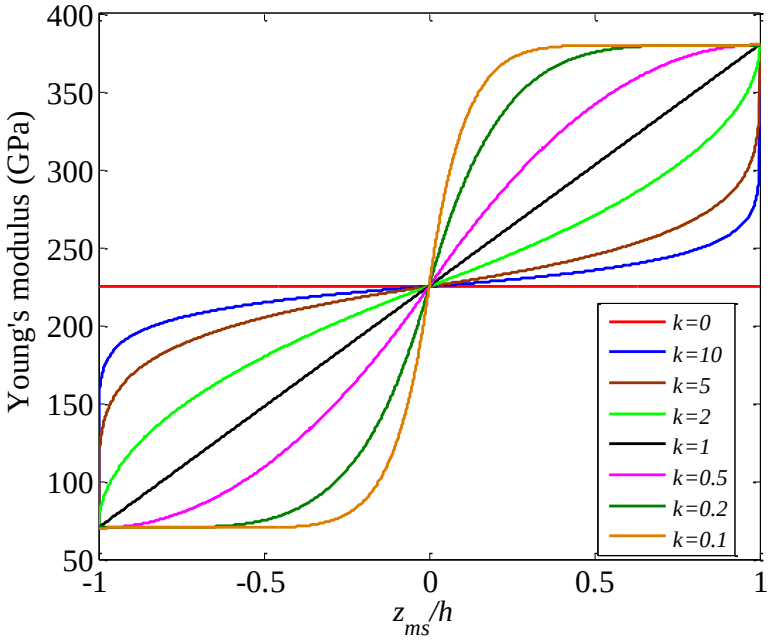

(a) Young's modulus.

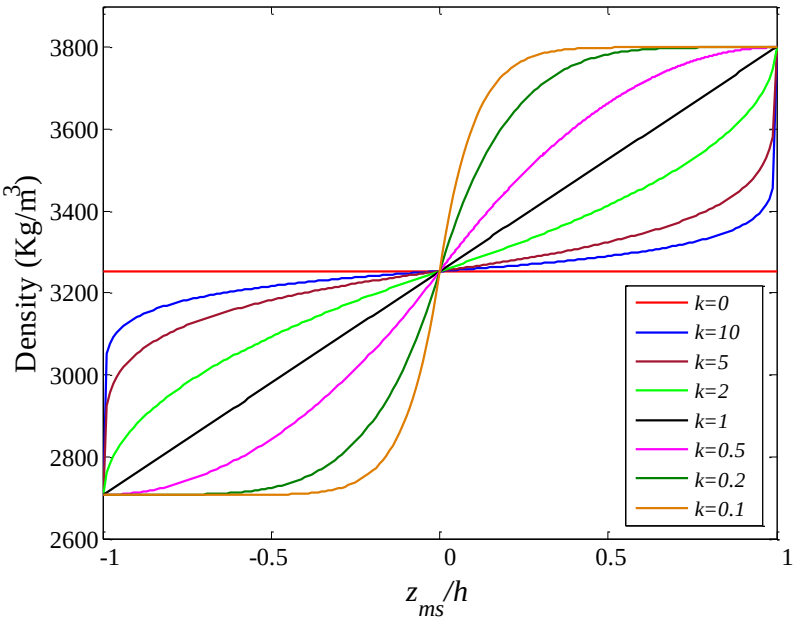

(b) Density

Fig. 2. The variation of Young's modulus (E) and density (ρ) of an S-FGM plate through thickness.

Figure

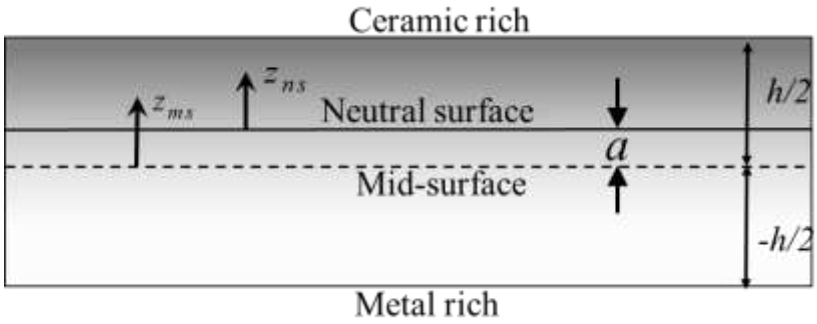

Fig. 3. The position of physical neutral surface and mid- surface for an S-FGM plate.

Figure

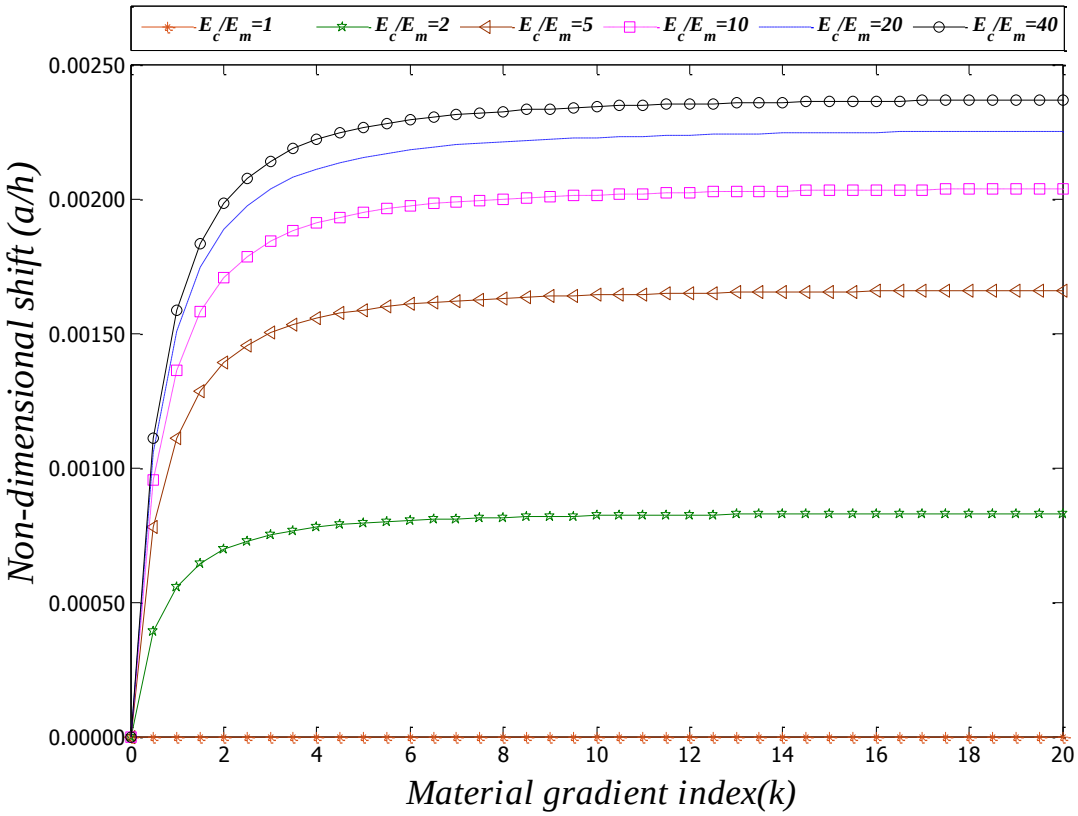

Fig. 4. The influence of the material gradient index on the non-dimensional shift (*a/h*)

Figure

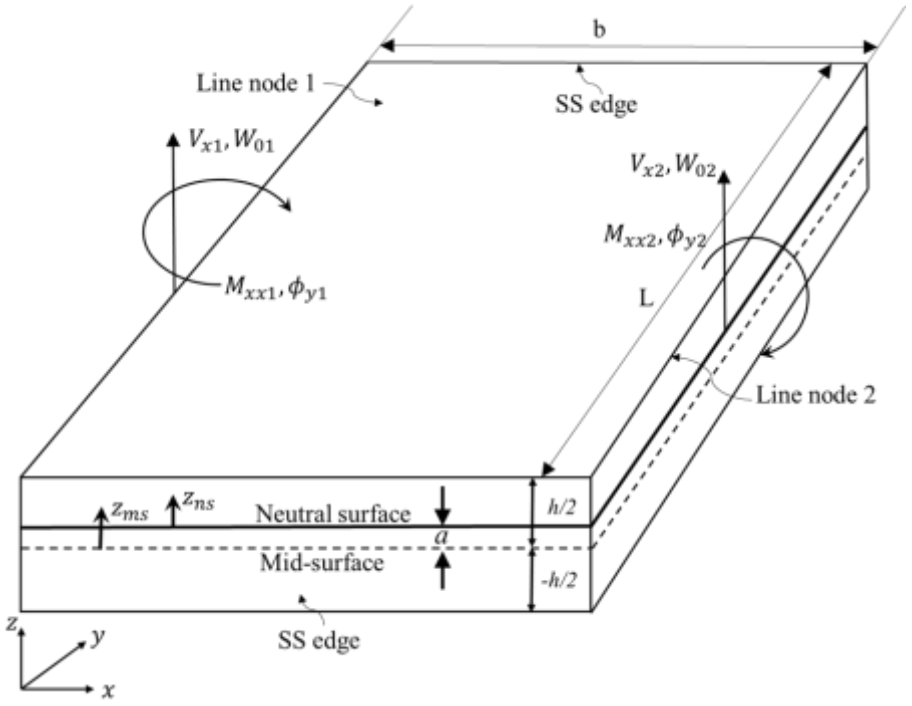

Fig. 5. Sign conventions for forces and moments of the S-FGM plate element

Figure

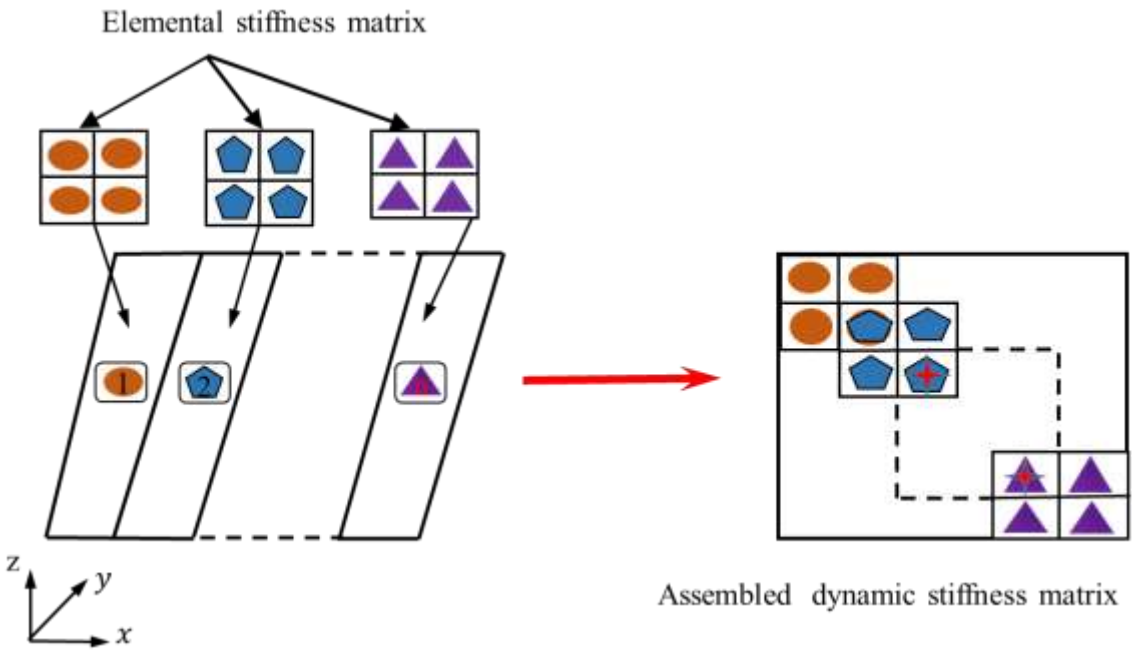

Fig. 6. Assembly procedure for DSM.

Figure

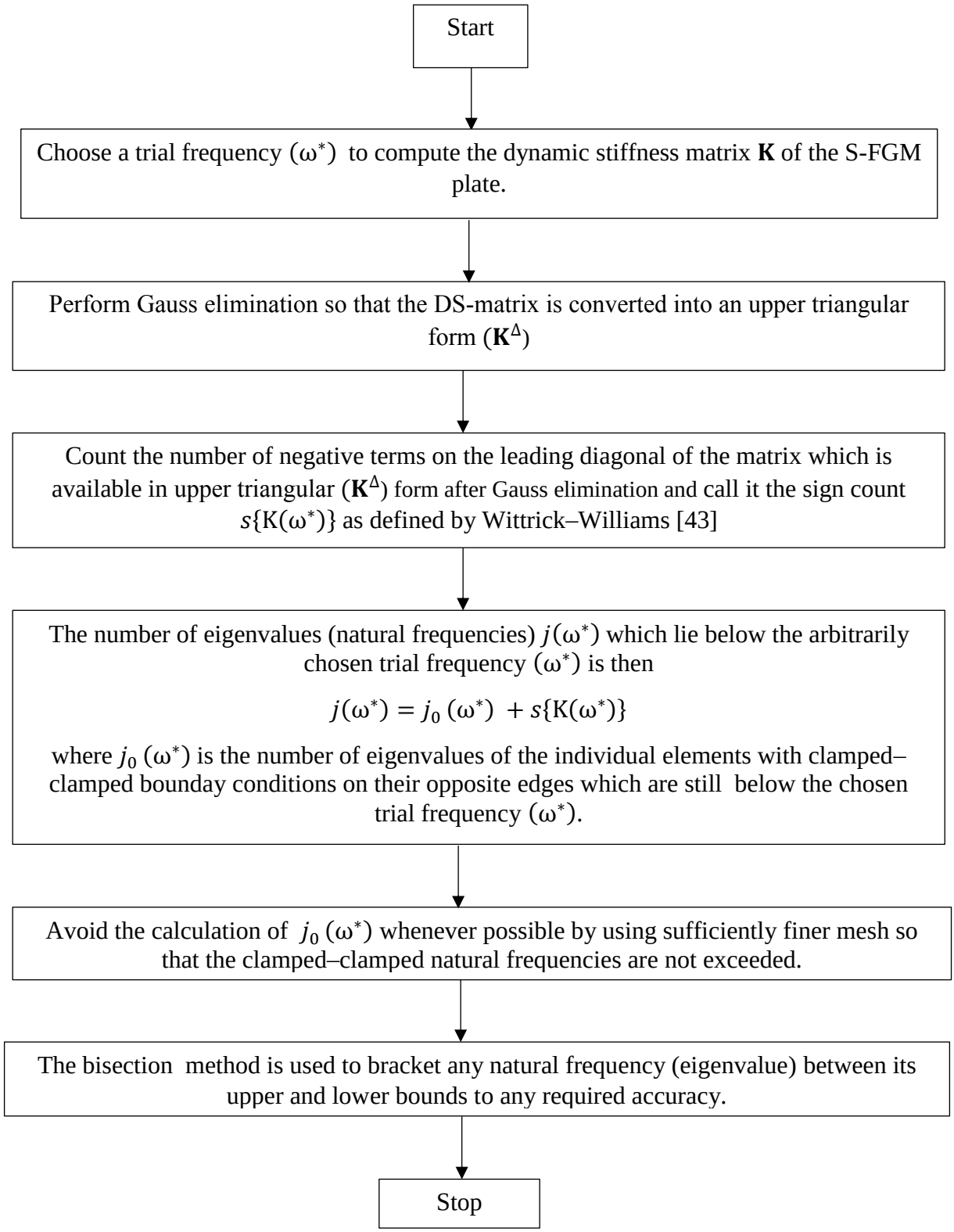

Fig. 7. Computational steps in implementing the Wittrick-Williams algorithm.

Figure

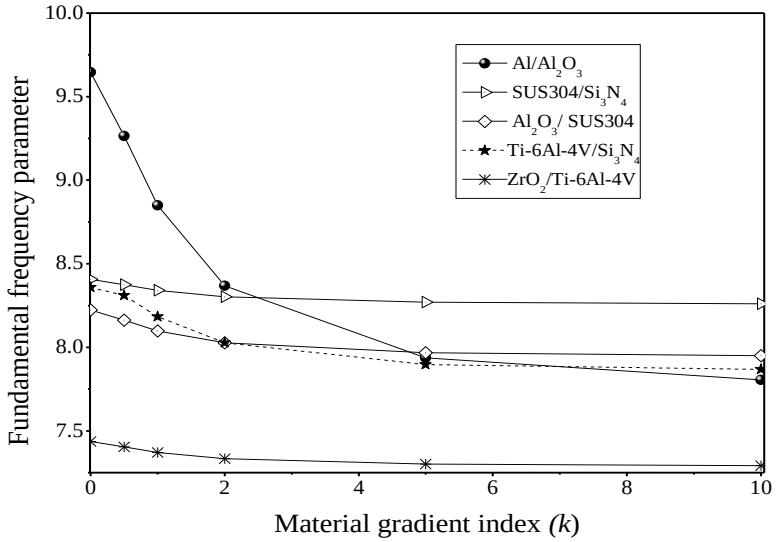

Fig. 8. Variation of fundamental natural frequency parameter versus material gradient index (*k*) of S -FGM plate made of different pairs of materials.

Figure

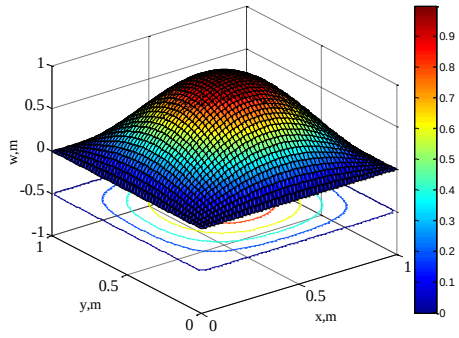

Natural mode (m =1, n =1)

$\bar{\omega} = 0.000477$

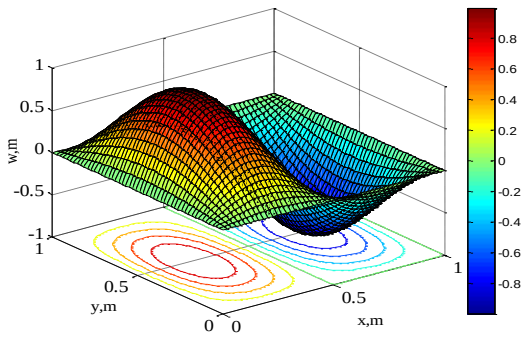

Natural mode (m =1, n =2)

$\bar{\omega} = 0.001193$

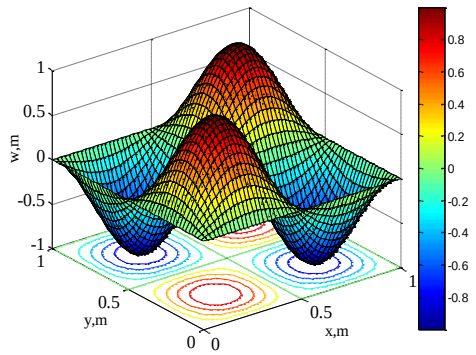

Natural mode (m =2, n =2)

$\bar{\omega}$ =0.001909

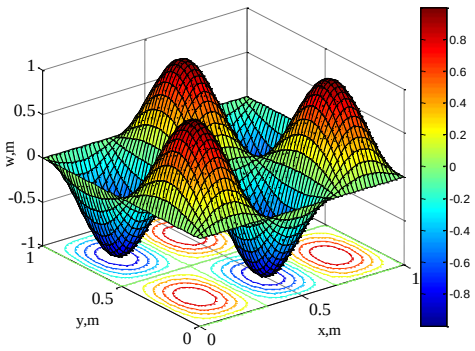

Natural mode (m =2, n =3)

$\bar{\omega} = 0.003102$

Fig. 9. Mode shapes of S-FGM square plate under the SSSS edge condition for k=0.5 and h/L=0.01.

Figure

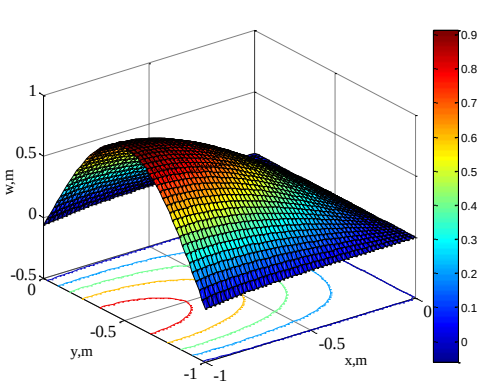

Natural mode (m =1, n =1)

$\bar{\omega} = 0.000299$

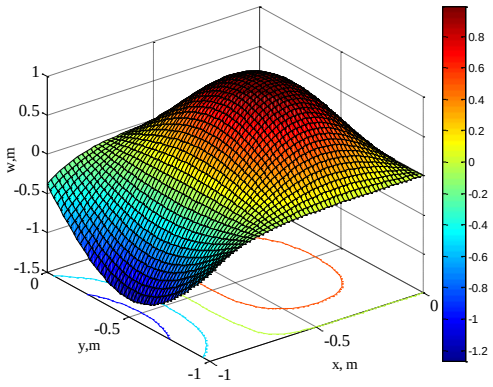

Natural mode (m =1, n =2)

$\bar{\omega} = 0.000711$

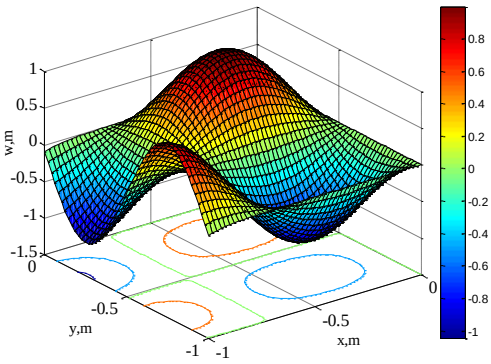

Natural mode (m =2, n =2)

$\bar{\omega} = 0.001513$

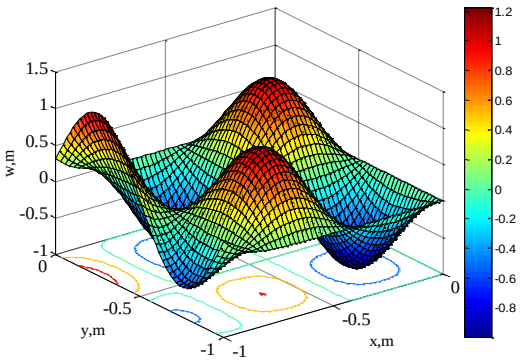

Natural mode (m =2, n =1)

$\bar{\omega} = 0.002421$

Fig 10. Mode shapes of S-FGM square plate under SFSS edge condition for k=0.5 and h/L=0.01

Figure

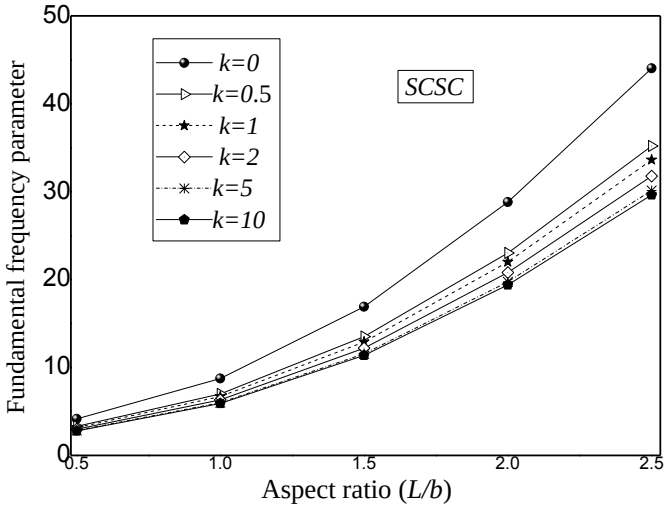

Fig.11 (a). Fundamental natural frequency parameter ($\bar{\omega}_1$) versus *L/b* ratio of S-FGM plate for different material gradient index (*k*) at a given *h/L* ratio of 0.01 under SCSC boundary condition

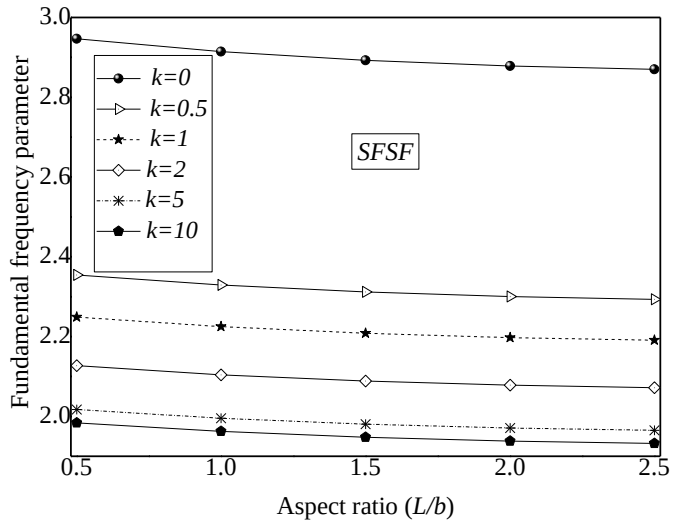

Fig. 11(b). Fundamental natural frequency parameter ($\bar{\omega}_1$) versus *L/b* ratio of S-FGM plate for different material gradient index (*k*) at a given *h/L* ratio of 0.01 under SFSF boundary condition.

Figure

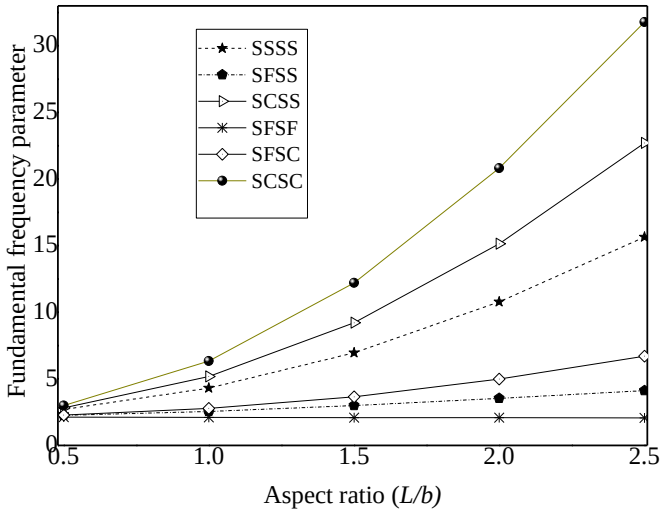

Fig. 12. Fundamental natural frequency parameter ($\bar{\omega}_1$) versus *L/b* ratio of S-FGM plate at a given *h/L* ratio of 0.01 and *k*=2 under different combinations of boundary conditions.

Figure

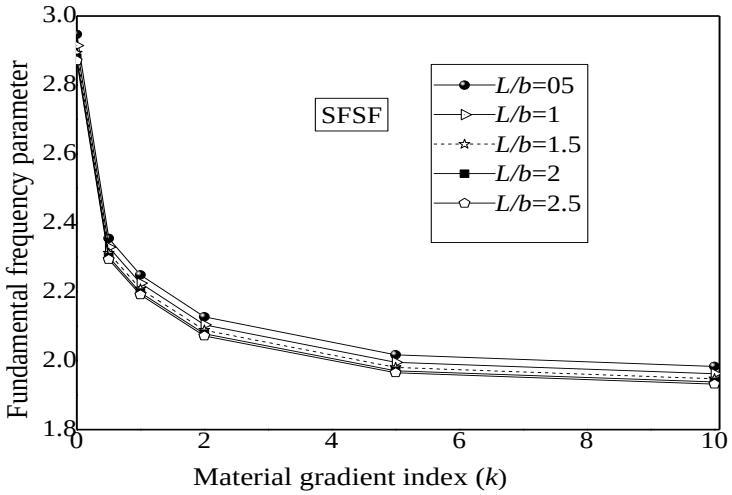

Fig. 13 (a). Fundamental natural frequency parameter ($\bar{\omega}_1$) versus material gradient index (k) of a rectangular S-FGM plate with h/L=0.01 for SFSF boundary condition.

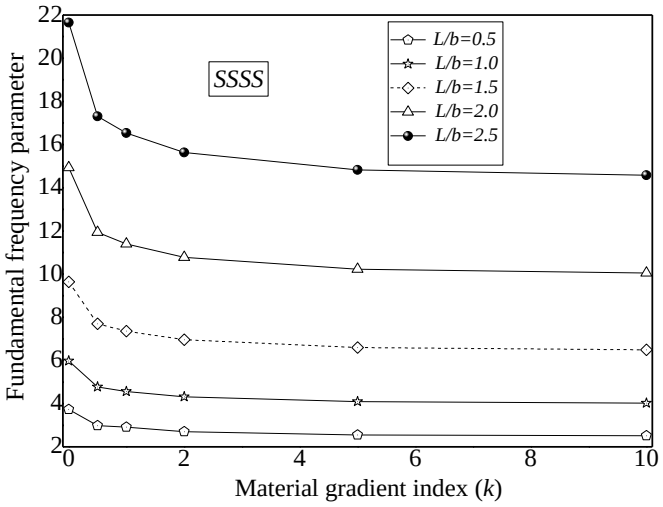

Fig. 13 (b). Fundamental natural frequency parameter ($\bar{\omega}_1$) versus material gradient index (k) of rectangular S-FGM plate with h/L=0.01 for SSSS boundary condition.

Figure

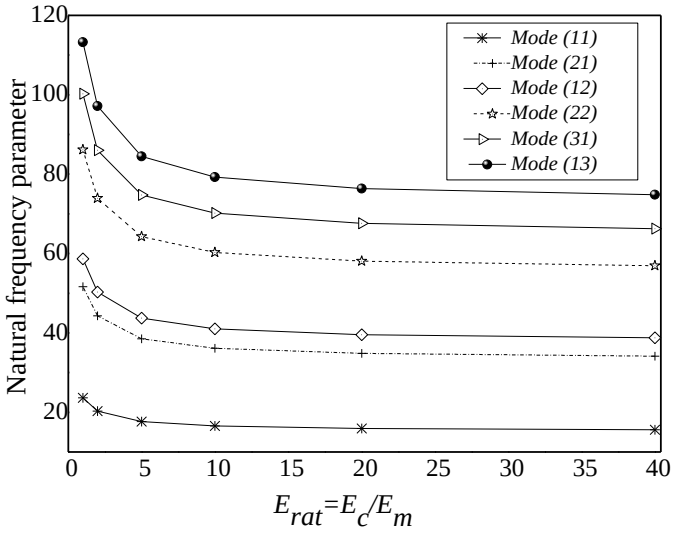

Fig. 14. Effect of E_{rat} on the natural frequency parameter ($\bar{\omega}$) of squre S- FGM plate for a given k=0.5 under SCSS boundary condition.

Figure

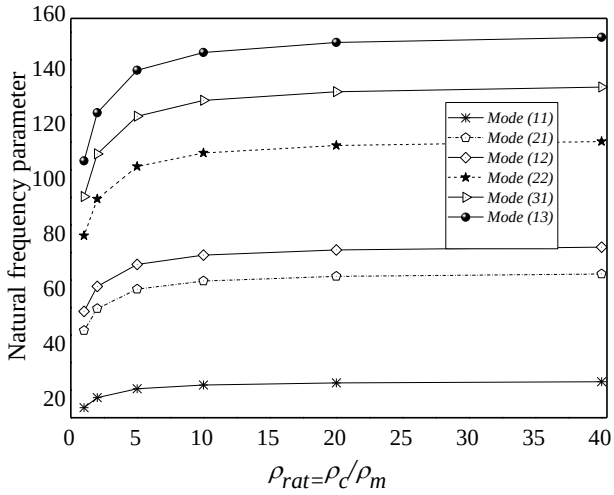

Fig. 15. Effect of ρ_{rat} on the natural frequency parameter ($\bar{\omega}$) of squre S- FGM plate for a given *k*=0.5 under SCSS boundary condition.

Figure

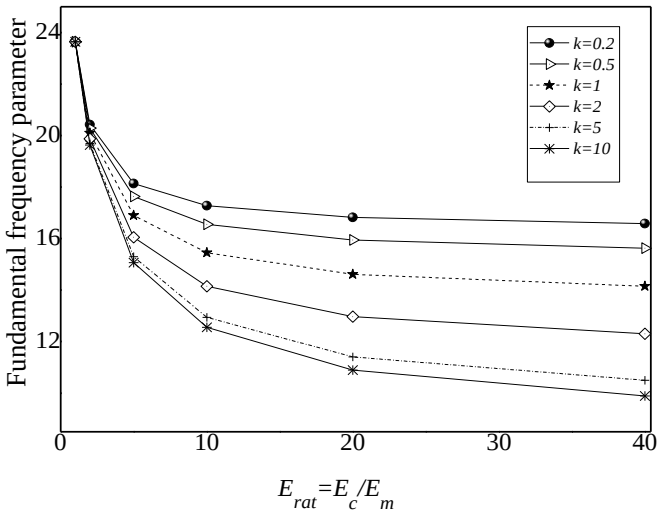

Fig. 16. Effect of different E_{rat} and constant ρ_{rat} on the fundamental natural frequency parameter ($\bar{\omega}_1$) of a square S- FGM plate with SCSS boundary condition for different material gradient index (k) and h/L =0.01.

Figure

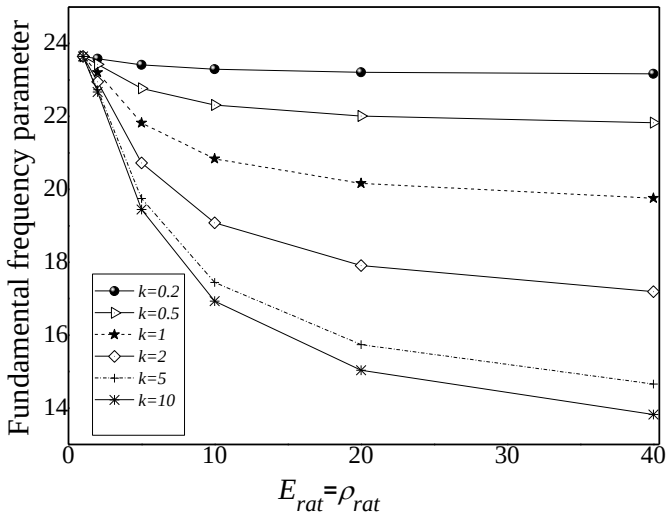

Fig. 17. Effect of $E_{rat} = \rho_{rat}$ on the fundamental natural frequency parameter ($\bar{\omega}_1$) of a square S-FGM plate with SCSS boundary condition for different material gradient index (k) and h/L =0.01.

Figure

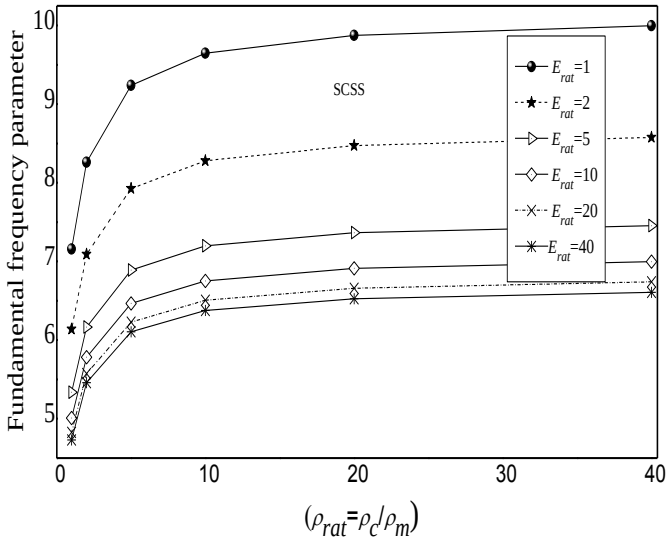

Fig. 18. Effect of density ratio ρ_{rat} on the fundamental natural frequency parameter $(\bar{\omega}_1)$ of a square S- FGM plate with SCSS boundary condition for different E_{rat} and k = 0.5 and *h/L* = 0.01

Table

Table

Table

Table

Table

Table